Estimating Mean Bedload Transport Rates and Their Uncertainty

Christophe Ancey[1] and **Ivan Pascal[1]**

[1]Ecole Polytechnique Fdrale de Lausanne, Lausanne, Switzerland

Measuring bedload transport rates usually involves measuring the flux of sediment or collecting sediment during a certain interval of time Δt. Because bedload transport rates exhibit significant non-Gaussian fluctuations, their time-averaged rates depend a great deal on Δt. We begin by exploring this issue theoretically within the framework of Markov processes. We define the bedload transport rate either as the particle flux through a control surface or as a quantity related to the number of moving particles and their velocities in a control volume. These quantities are double averaged; that is, we calculate their ensemble and time averages. Both definitions lead to the same expression for the double-averaged mean rate and to the same scaling for the variance's dependence on the length of the sampling duration Δt. These findings lead us to propose a protocol for measuring double-averaged transport rates. We apply this protocol to an experiment we ran in a narrow flume using steady-state conditions (constant water discharge and sediment feed rates), in which the time variations in the particle flux, the number of moving particles, and their velocities were measured using high-speed cameras. The data agree well with the previously defined theoretical relationships. Lastly, we apply our experimental protocol to other flow conditions (a long laboratory flume and a gravel-bed river) to show its potential across various contexts.

1. Introduction

1.1. Bedload Transport Rate and Fluctuations

Whether measuring bedload transport rates in the field or the laboratory, we are faced with a three-part problem. First, there is no universally accepted definition of the bedload transport rate Q_s, and various definitions have been used depending on the context (Ballio et al., 2014, 2018; Furbish et al., 2017). For instance, in the laboratory, it has long been common to collect the sediment transported to the flume outlet over a given time interval and weigh it to deduce a time-averaged value of Q_s. Today, techniques based on impact plates, acoustic sensors and image processing enable high-frequency measurements of Q_s (Geay et al., 2017; Gray et al., 2010; Mendes et al., 2016; Rickenmann et al., 2014; Singh et al., 2009; Tsakiris et al., 2014). In both cases, Q_s is defined as the particle flux through a surface. Alternatively, in the field, using tagged particles (tracers) has long been the simplest way of measuring transport rates (Wilcock, 1997), with Q_s reflecting the complex history of the particles entrained by the flow and subsequently deposited (or possibly buried) on the streambed (Einstein, 1950). Second, measuring sediment transport rates (i.e., the displacements and velocities of sediment, and the number of moving particles) remains an enormous technical challenge. Geophones and seismic sensors can only provide proxy calculation methods, which can be related to Q_s after signal processing (Gray et al., 2010). Discriminating between the various processes (multiple impacts, differently sized sediment, rolling or saltating sediment) is fraught with difficulty (Dhont et al., 2017; Dietze et al., 2019; Wyss et al., 2016). Third, recorded transport rates exhibit very significant non-Gaussian fluctuations even under steady-state flow conditions (Ancey & Heyman, 2014; Ancey et al., 2008). When both the sediment feed rate and water discharge vary over time, it becomes extremely difficult to separate the various random particle movement and bedform migration components of fluctuation and to disentangle the time scales associated with each process (Dhont & Ancey, 2018).

Although the existence of wide fluctuations in bedload transport rates—and their influence on their mean rate estimates—has long been known (Bunte & Abt, 2005; Gomez, 1991; Recking et al., 2012; Singh et al., 2009), some scientists show little awareness of the crucial influence of measurement protocols, particularly the definition of sampling duration, when estimating mean transport rates and their associated uncertainties. Very few experimental papers have specified how accurate their bedload transport rate measurement was. In many cases, authors mentioned that because they had achieved steady-state conditions, collecting
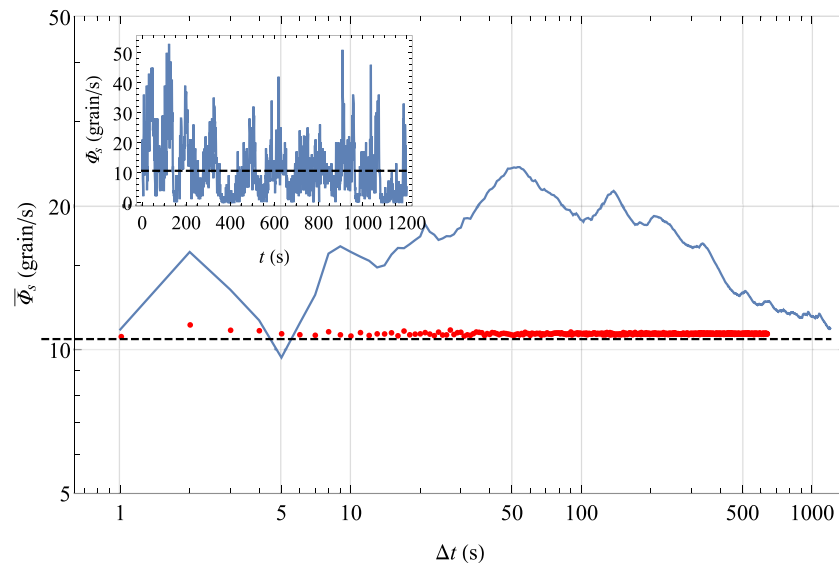
Figure 1. Variation in the time-averaged particle flux (solid line) $\Phi_s = (\Delta t)^{-1} \int_0^{\Delta t} \Phi_s(t) dt$ with sampling duration Δt. The instantaneous particle flux $\Phi_s(t)$ was measured by counting the number of particles crossing a control surface located at the flume outlet during a time interval $\delta t = 4$ ms. The flume was 2.5 m long and tilted at 1.55° to the horizontal (see section 3 for further information on the experiment). The horizontal dashed black line shows the feed rate $Q_{in} = 10.3$ grains/s. The inset shows the time variations in the instantaneous particle flux Φ_s. The red dots show the mean particle fluxes computed using our proposed protocol based on the bootstrap method (see section 2.7).

sediment at the flume outlet over durations of 1 min or so was sufficient to obtain the mean transport rate. Setting an arbitrary sampling duration is, however, seldom satisfactory. Figure 1 provides a typical example of how sensitive the time-averaged particle flux $\overline{\Phi}_s$ is to sampling durations (see the caption of Figure 1 or Equation 1 for the definition of $\overline{\Phi}_s$). The mean particle flux was measured in the middle of the flume using image processing (see sections 3 and 4 for further information). Although the feed rate Q_{in} was constant at the flume inlet (set to 10.3 grains/s), the instantaneous particle flux exhibited fluctuations as large as $5Q_{in}$, causing the time-averaged particle flux $\overline{\Phi}_s$ to deviate substantially from its steady-state value Q_{in}. Convergence toward the steady-state value Q_{in} was quite slow: sampling durations should exceed 20 min to get the mean particle flux to within 5%; with other flumes and experimental conditions, we had to wait 100 hr (Dhont & Ancey, 2018). Thus, although it has often been overlooked in research papers to date (Ancey, 2020), we believe that proper estimation of the uncertainties associated with bedload transport measurements should be a central issue in any experimental protocol.

The uncertainty principles in physics (e.g., Heisenberg's principle) and signal processing (e.g., Gabor's principle) set limits to the precision with which certain physical properties can be measured simultaneously. One can intuitively understand that calculating bedload transport also involves a trade-off between the level of noise and the representativeness of time-averaging: if a short sampling duration is selected, the time-averaged flux $\overline{\Phi}_s$ is representative of the mean local bedload transport rate, but it is also associated with a lot of noise ($\overline{\Phi}_s$ variance is large). On the contrary, if a long sampling duration is selected, the variance of $\overline{\Phi}_s$ is small, but $\overline{\Phi}_s$ may be biased, especially under time-dependent flow conditions (Ballio et al., 2014).

1.2. Objectives

The present paper proposes a method for estimating the average and variance of a particle transport rate Q_s when a Q_s time series is available. We consider two definitions of bedload transport rate (see section 2): first, measuring a particle flux through a control surface (e.g., using geophones or image processing) or second, measuring particle displacements and velocities in a control window (e.g., using a high-speed camera or an acoustic Doppler velocimetry profiler). We are aware that these definitions may not cover all conditions and measurement techniques, but at least they correspond to techniques commonly in use today. The theoretical underpinnings are based on the stochastic bedload transport model developed by Ancey et al.
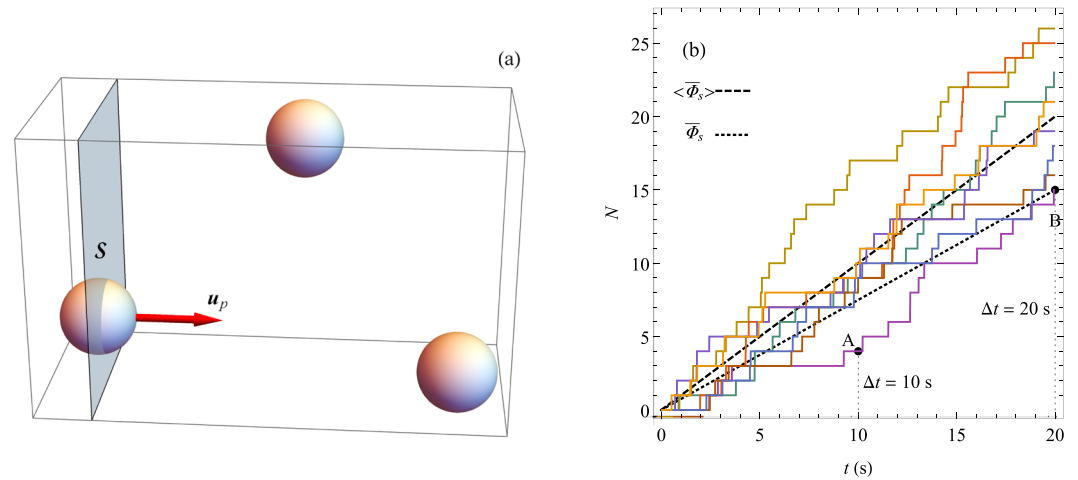
Figure 2. (a) Illustration of the virtual experiment: Particles move randomly at velocity $\boldsymbol{u}_p$ and cross the control surface $\mathcal{S}$. (b) Time variations in the number of particles $N(t)$ that have crossed the control surface $\mathcal{S}$ until time t. Here we simulated eight paths of the Poisson process $N(t)$ with rate $\nu = 1$ grains/s and a sampling rate $\delta t = 5$ ms (thus generating $M = 4{,}000$ values of N for each path).

(2008). When sufficient statistical information can be inferred from experimental data, an alternative to calculating the time-averaged particle flux is the use of renewal theory (see Appendix B). Both methods involve high-frequency measurement of the instantaneous transport rate (typically higher than 1 Hz). When high acquisition frequencies are impossible, the central limit theorem provides the asymptotic variation of the $\overline{q}_s$ variance with sampling duration Δt. This method has been successfully applied to various setups in well-controlled laboratory experiments (see section 4). We present two other applications to demonstrate that the proposed method can be used in various settings (see section 5).

1.3. A Toy Model

To give a foretaste of the ideas developed in this paper, we consider a virtual experiment. Particles arrive randomly in a flume at a rate $\nu = 1$ grain/s and cross a control surface $\mathcal{S}$ (see Figure 2a). By counting the number N of particles that have crossed $\mathcal{S}$ during the time interval Δt, we can estimate the mean particle flux as $\overline{\Phi}_s = N/\Delta t$. Because bedload transport exhibits large non-Gaussian fluctuations, even under steady-state conditions, we obtain different $\overline{\Phi}_s$ values depending on when we start the measurement or which path is selected. Figure 2b shows eight replicates from the same experiment: Particle arrival is described as a Poisson process (as we will see later, this is a fair assumption when bedload transport is weak), all paths are realizations of the Poisson process with rate $\nu = 1$ grain/s, and thus the number of particles crossing $\mathcal{S}$ over a time interval Δt varies from one run to another. If we consider the specific run whose endpoint is B (at time $t = 20$ s) in Figure 2b, we find that $N = 4$ for $\Delta t = 10$ s (point A), and thus $\overline{\Phi}_s = 4/10 = 0.4$ grains/s, a value 60% off the mean rate ν.

How can we improve accuracy? The simplest idea is to increase the time interval Δt. By taking $\Delta t = 20$ s, we find $N = 15$ (point B) and thus $\overline{\Phi}_s = 15/20 = 0.75$ grains/s. The error has dropped to 25%. This is consistent with what Bunte and Abt (2005) and Singh et al. (2009) showed in their field and laboratory experiments: the sample mean and variation vary with increasing sampling durations, and the longer the sampling duration, the lower the error. There are two problems with this approach. First, in practice, it is difficult to take long sampling durations, especially if the flow is time dependent. Second, when computing the time-averaged flux $\overline{\Phi}_s = N/\Delta t$, we have no idea how close this estimate is to the actual rate ν. Indeed, the sample variance is computed by using the Φ_s values along a particular path, and it does not tell us anything about the relative error $\varepsilon = |1 - \overline{\Phi}_s/\nu|$. For instance, for path AB, the sample variance is $\sigma_\Phi^2 = \sum_{k=1}^{M}(N(t) - \overline{\Phi}_s t)^2 = 3.72$ grains^2/s^2 (M is the number of sampled values), yielding a coefficient of variation $\sigma_\Phi/\overline{\Phi}_s = 12.8\%$, which is lower than the relative error $\varepsilon = 25\%$ by a factor 2.
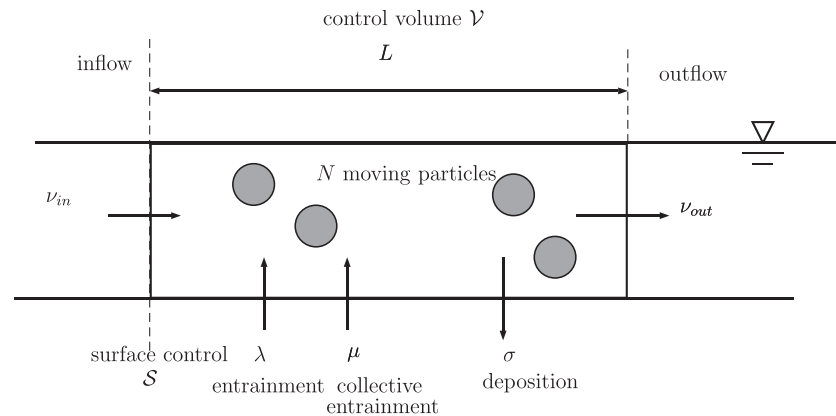
Figure 3. Notation and illustration of the exchange processes considered. The water flow transports particles. The mean particle flux is ν_{in}. The number of moving particles N in the control volume $\mathscr{V}$ varies as a result of particles entering and leaving the volume and being entrained or deposited on the bed. Bed particles can be dislodged by the water drag (there is a probability λdt that this occurs within a short time interval dt) or because of interactions with moving particles (as there are N moving particles, the resulting probability of entrainment is $\mu N dt$).

Another approach involves replicating the initial run to refine the estimate $\overline{\Phi}_s$. The average of the eight runs provides a mean rate $\overline{\Phi}_s = 0.95$ grain/s for $\Delta t = 10$ s, and $\overline{\Phi}_s = 1.02$ grain/s for $\Delta t = 20$ s, with the relative error thus dropping to 2–5%. This shows that by combining time and run averages, we can reduce uncertainties when measuring bedload transport. Run averaging is close to ensemble averaging $\langle \overline{\Phi}_s \rangle = \lim_{n \to \infty} \sum_{i=1}^{n} N/\Delta t$, which is the tool we will be using in this paper. At this stage of the example, one might doubt that much progress has been made if, in practice, one has to reiterate measurements instead of extending the sampling duration Δt. This is where theory comes in.

We will show that uncertainties (expressed here in terms of ensemble-variance var $\overline{\Phi}_s$) vary as var $\overline{\Phi}_s = K/\Delta t$. The proportionality factor K depends on the measurement protocol and transport stage. When measuring low transport rates, K is equal or close to the mean flux $\overline{\Phi}_s$. If we go back to the example in Figure 2 and consider path AB again, we measure $\overline{\Phi}_s = 15/20 = 0.75$ grains/s, thus deducing that the ensemble variance is approximated by var $\overline{\Phi}_s = \overline{\Phi}_s/\Delta t = 0.0375$ grains^2/s^2 and expecting the actual rate to fall within or close to the range $\overline{\Phi}_s \pm \sqrt{\text{var } \overline{\Phi}_s} = [0.56, \, 0.94]$ grains/s. The ensemble-averaged variance var $\overline{\Phi}_s$ thus provides a better estimate of the uncertainties of $\overline{\Phi}_s$ than the sample mean.

We have been able to estimate the ensemble-averaged variance from a single path because we have taken advantage of our knowledge of sediment transport: It behaves like a Markov process at low transport rates. At higher transport rates, the assumption of a Markov process breaks down, but our statistical approach is still possible. It requires more statistical information about $\overline{\Phi}_s$ to implement renewal theory and determine the value of K. High-resolution data were needed for this. Admittedly, replicating measurements is usually difficult (and often impossible), but we will see that statistical techniques such as bootstrapping allow us to estimate the ensemble mean and variance. In the absence of high-resolution data, applying the central limit theorem provides an estimate of K.

2. Theory

2.1. Definitions and Notation

The present paper uses two different definitions of the bedload transport rate Q_s from among the numerous forms currently in use (Ancey, 2010; Ballio et al., 2014; Furbish et al., 2012). We have tailored these definitions to the specific analysis developed in this paper (see the end of this section for how these definitions can be generalized in real-world applications). First, for most theoretical developments, we will express Q_s in grains/s. Second, we will consider a flow per unit width. Although many of the equations presented seem to have been formulated for a two-dimensional problem, the third spatial dimension should not be forgotten.

For this reason, we will refer to "control volume" even though this volume is two-dimensional in Figure 3 (the same holds for the control surface and streambed area below).

- Flux of particles across a control surface (see Figure 3). We count the number of particles crossing the control surface $\mathcal{S}$ during the sampling duration Δt:

$$\overline{\Phi}_s(\Delta t|t) = \frac{1}{\Delta t}\int_t^{t+\Delta t}\phi_s(\tau)\mathrm{d}\tau, \tag{1}$$

where $\varphi_s(\tau)\mathrm{d}\tau$ gives the number of particles intersecting the control surface $\mathcal{S}$ between time τ and $\tau+\mathrm{d}\tau$. Thereafter, we will mostly work with Markov processes that describe weak sediment transport: In such cases, the probability of observing two particles crossing the control surface at the same time drops to zero, and $\varphi_s\mathrm{d}\tau$ can either be zero (no particle crossing $\mathcal{S}$) or unity (one particle crossing $\mathcal{S}$). The arrival of individual particles will be described as a Poisson process in section 2.3. When this assumption breaks down at sufficiently high transport rates, φ_s can take any integer value, and we describe particle arrival as a renewal process (see Appendix B). Equation 1 is probably the most natural definition in fluid mechanics because particle transport rates usually reflect mass fluxes. Indeed, it is equivalent to the definition used in continuum mechanics $\mathcal{Q}_s = \int_{\mathcal{S}} H(\boldsymbol{x})\boldsymbol{u}_p(\boldsymbol{x},\,t)\cdot\boldsymbol{n}\mathrm{d}S$ (where $H(\boldsymbol{x})$ is unity when point $\boldsymbol{x}$ is occupied by a particle and zero otherwise, $\boldsymbol{u}_p$ is the particle velocity field at $\boldsymbol{x}$, and $\boldsymbol{n}$ is the outward-oriented normal to $\mathcal{S}$).

- Volume-averaged particle transport rate. By averaging particle motion through a control volume, we relate the bedload transport rate to the volume-averaged particle velocity $\mathcal{U}_p = \sum_{i=1}^{N} u_{p,i}$ (where $u_{p,i}$ is the instantaneous particle velocity) and the number of moving particles N (Ancey & Heyman, 2014):

$$q_s = \frac{N}{A}\mathcal{U}_p, \tag{2}$$

where N/A is called the *particle activity* (i.e., the number of moving particles per unit of streambed area A) (Furbish et al., 2012). Counting the number of moving particles and determining their mean velocity leads to the instantaneous volume-averaged transport rate q_s. We can calculate its time average:

$$\overline{q}_s(\Delta t|t) = \frac{1}{\Delta t}\int_t^{t+\Delta t}q_s(\tau)\mathrm{d}\tau, \tag{3}$$

where Δt is the sampling duration. If we assume that particles move at a constant velocity, then computing the bedload transport rate involves determining the number of moving particles N. Calculating the time-averaged bedload transport rate $\overline{q}_s$ is tantamount to calculating the time integral of $N(t)$. This is what we will do below by using some general results for Markov processes (see Appendix A) and by applying renewal theory (see Appendix B).

We introduce three averages:

- The *ensemble average* $\langle f\rangle$ of the random quantity f is obtained by averaging f over all possible realizations (Drew & Passman, 1999; Herczynski & Pienkowska, 1980; Lhuillier, 1992)—the electronic supplement to Ancey and Heyman (2014) provides a more formal introduction to this average. If f depends on time t, then $\langle f\rangle$ is also a function of t. We denote the steady-state ensemble-averaged value of f by $\langle f\rangle_{\mathrm{ss}}$, which is the value reached by $\langle f\rangle$ at sufficiently long time intervals for the initial condition's influence to be negligible.
- The time average $\overline{f}$ is defined as the time integral over the sampling duration Δt:

$$\overline{f}(\Delta t|t) = \frac{1}{\Delta t}\int_t^{t+\Delta t}f(\tau)\mathrm{d}\tau. \tag{4}$$

- We can combine both averages to produce the double-averaged (time- and ensemble-averaged) quantity $\langle\overline{f}\rangle$.

To keep the notation less cluttered, we did not introduce any special symbol to refer to the volume average underpinning the derivation of Equation 2. When sediment transport involves grains of the same size, we can readily convert transport rates expressed in grains/s into rates expressed in kg/s or m^3/s. When considering grains of different sizes, the definitions (1) and Equation 3 can be generalized by partitioning the grain size distribution into classes and computing particle transport rates for each class.

2.2. Assumptions

We consider a one-dimensional system under steady-state conditions, corresponding to a narrow, tilted flume with a constant feed rate at its inlet (the flow geometry that will be investigated experimentally in section 4). Under these flow conditions, particles move in the same direction as the water flow, and cross-stream diffusion—observed in wider flumes (Seizilles et al., 2014)—can be neglected. The influence of bedforms on flow dynamics and bedload transport is supposed to be negligible, and thus the bed is in equilibrium with no significant elevation variation along its interface with the flow (neither aggradation nor degradation). Particles move at velocity u_p, which may fluctuate over time. The mean particle velocity is denoted by $\bar{u}_p$. Velocity fluctuations are assumed to be Gaussian, with standard deviation σ_u. The probability P_u of observing a given value w for the particle velocity is thus

$$P_u(w) = \text{prob } (u = w) = \frac{1}{\sqrt{2\pi}\sigma_u} \exp\left(-\frac{(w-\bar{u}_p)^2}{2\sigma_u}\right). \tag{5}$$

This assumption has been validated experimentally (Ancey & Heyman, 2014; Heyman et al., 2016; Martin et al., 2012), but not systematically; authors have observed an exponential velocity distribution instead (Lajeunesse et al., 2010; Roseberry et al., 2012). The exact form is not crucial to the rest of the developments.

The central element of our theoretical development is the calculation of the number N of particles crossing a control surface or contained in a control volume. To that end, we use the stochastic bedload transport model proposed by Ancey et al. (2008). The number of moving particles N varies with time as a result of (i) deposition and (ii) entrainment. Particles come to rest at a rate σ [1/s]. The *deposition rate D* is thus $D = \sigma N$ [grains/s]. We introduce two forms of entrainment:

- *Individual entrainment* at a rate λ [grains/s], which reflects the classic mechanism of entrainment by the water flow.
- *Collective entrainment* at a rate μ [1/s], which takes particle–particle interactions into account.

The number of particles entrained per unit time is thus $E = \lambda + \mu N$, where E is the *entrainment rate* [grains/s]. To accurately count particles, the system's dimensions must be specified. We consider a control window $\mathcal{V}$ of length L. The window's downstream (or equivalently, upstream) face is the control surface $\mathcal{S}$ (see Figure 3).

We assume that the particle flux can be described as a Markovian process. This implies that the probability of observing N moving particles depends only on recent flux history (there is no memory effect). Differently put, the probability P that one particle crosses the control surface $\mathcal{S}$ during the time interval $[t,t+\delta t]$ is $P = \nu_{\text{in}}\delta t$ (where ν_{in} is the feed rate), and thus that probability depends solely on the time interval δt. When δt is infinitesimally small, then only one particle can cross the control surface (Markovian process theory cannot deal with multiple events). Equivalently, it can be shown that the waiting time τ between two particle-arrivals is exponentially distributed, with parameter $\Lambda = \nu_{\text{in}}$ [grains/s] (or equivalent with a mean waiting time $t_w = \nu_{\text{in}}^{-1}$):

$$P_\tau(\tau) = \Lambda\exp(-\Lambda\tau). \tag{6}$$

2.3. Time-Averaged Particle Flux

With these assumptions, we deduce immediately that the number of particles that have crossed the control surface $\mathcal{S}$ up to time t is a Poisson process (Cox & Miller, 1965; Gillespie, 1992). It is straightforward to show that the ensemble average and variance are (Gillespie, 1992)

$$\langle N \rangle = \Lambda t \quad \text{and} \quad \text{var } N = \Lambda t. \tag{7}$$

Using Equation 1, we then deduce that the mean (double-averaged) flux is

$$\langle \overline{\Phi}_s \rangle (\Delta t|t) = \frac{\langle N \rangle (t + \Delta t) - \langle N \rangle (t)}{\Delta t} = \Lambda, \tag{8}$$

regardless of Δt, whereas the variance is

$$\text{var }\overline{\Phi}_s(\Delta t|t)=\frac{\Lambda}{\Delta t}. \tag{9}$$

Interestingly, we note that according to the Poisson process, the fluctuation strength varies linearly with the mean particle flux Λ and is inversely proportional to the sampling duration Δt.

2.4. Volume-Averaged Bedload Transport Rate for $\sigma_u = 0$

Let us first consider the simplest case, in which the particle velocity fluctuations are negligible relative to their mean velocity $\bar{u}_p$ (i.e., we assume that $\sigma_u = 0$). The number N of moving particles in the control window $\mathscr{V}$ can be described as a birth-death immigration-emigration Markov process (Cox & Miller, 1965): entrainment and deposition correspond to birth and death, respectively, whereas immigration and emigration reflect the arrival and departure of particles. The immigration rate is ν_{in}, and the emigration rate is

$$\nu_{\text{out}}=\frac{\bar{u}_p}{L}, \tag{10}$$

where L is the length of the control window. Under steady-state conditions, the probability of observing N particles in the control volume $\mathscr{V}$ can be calculated analytically. Here we summarize the main results and refer the reader to an earlier publication for the proofs (Ancey et al., 2008).

When the collective entrainment rate μ is nonzero, this probability is the negative binomial distribution:

$$P_n(n)=\text{prob }(N=n)=\binom{cq+n-1}{q-1}p^q(1-p)^n \tag{11}$$

with parameters p and q:

$$q=\frac{\lambda+\nu_{\text{in}}}{\mu}\quad\text{and}\quad p=1-\frac{\mu}{\nu_{\text{out}}+\sigma-\mu} \tag{12}$$

The autocorrelation function of the time series $N(t)$ is

$$\rho(\tau|t)=\frac{\text{cov }(N(t),N(t+\tau))}{\text{var }N(t)}=e^{-\tau/t_c}, \tag{13}$$

where $t_c = 1/(\nu_{\text{out}}+\sigma-\mu)$ is the autocorrelation time. Under steady-state conditions, the ensemble average and mean of N are thus

$$\langle N\rangle_{\text{ss}}=\frac{\lambda+\nu_{\text{in}}}{\nu_{\text{out}}+\sigma-\mu}\quad\text{and}\quad\text{var}_{ss}\,N=\frac{(\lambda+\nu_{\text{in}})(\nu_{\text{out}}+\sigma)}{(\nu_{\text{out}}+\sigma-\mu)^2}. \tag{14}$$

The instantaneous bedload transport in the control volume $\mathscr{V}$ is given by Equation 2. As we assume that particles move at constant velocity $\bar{u}_p$, then all the q_s fluctuations result solely from the time variations in the number of moving particles N. Combining Equations 2 and 14, we find that under steady-state conditions, the ensemble-averaged bed transport rate is

$$\langle q_s\rangle_{\text{ss}}=\frac{\bar{u}_p}{L}\langle N\rangle_{\text{ss}}=\frac{\lambda+\nu_{\text{in}}}{\nu_{\text{out}}+\sigma-\mu}\frac{\bar{u}_p}{L}. \tag{15}$$

Because under steady-state conditions we have $\bar{u}_p\langle N\rangle_{\text{ss}}/L=\nu_{\text{in}}=\Lambda$, the steady-state mean transport rate (15) matches the mean particle flux (8). The variance takes a more complicated form:

$$\text{var}_{ss}\,q_s=\frac{\bar{u}_p^2}{L^2}\text{var}_{ss}\,N=\frac{\bar{u}_p^2(\lambda+\nu_{\text{in}})(\nu_{\text{out}}+\sigma)}{L^2}\frac{}{(\nu_{\text{out}}+\sigma-\mu)^2}. \tag{16}$$

Calculating the double-averaged bedload transport rate $\langle\bar{q}_s\rangle$ requires more work. First, we can derive the governing equation specific for $\langle N(t)\rangle$, its higher moments, and its time integral $\int_t N(t)\text{d}t$ (see Appendix A

for the mathematical detail). By using Equation A19 and assuming that particles were initially still $(N_0 = N(t = 0) = 0)$ in the control volume, we find that

$$\langle \overline{q}_s \rangle (\Delta t | t) = \frac{\overline{u}_p}{L} \frac{\lambda + \nu_{\text{in}}}{\nu_{\text{out}} + \sigma - \mu} \left(1 - \frac{t_c}{\Delta t} (1 - e^{-\Delta t / t_c}) \right), \tag{17}$$

which tends to $\langle q_s \rangle_{\text{ss}}$ when the sampling duration Δt is sufficiently long relative to the autocorrelation duration t_c. Asymptotically, the variance is deduced by taking the limit $\Delta t \gg t_c$ in Equation A22:

$$\text{var } \overline{q}_s(\Delta t | t) = \frac{\overline{u}_p^2}{L^2 \Delta t} \frac{(\lambda + \nu_{\text{in}})(\nu_{\text{out}} + \sigma)}{(\nu_{\text{out}} + \sigma - \mu)^3} = \frac{\overline{u}_p^2}{L^2} \text{var}_{ss} \, N \frac{t_c}{\Delta t}. \tag{18}$$

Contrary to the average (17), the double-averaged variance does not converge to the steady-state ensemble-averaged variance (16) when $\Delta t \gg t_c$. We also note that, contrary to the particle flux, the fluctuation strength depends on many parameters and does not seem to be trivially related to the mean bedload transport rate. The particle flux, however, is inversely proportional to the sampling duration. We can intuitively estimate that the proportionality factor $\overline{u}_p^2 \text{var}_{ss} N t_c / L^2$ in Equation 18 should be close to Λ. As shown in section 4, this link between $\overline{u}_p^2 \text{var}_s N t_c / L^2$ and Λ was observed experimentally, but we have no theoretical argument with which to rigorously demonstrate it.

2.5. Volume-Averaged Bedload Transport Rate for $\sigma_u > 0$

Calculations become more involved when considering velocity fluctuations, but they are still tractable analytically. We assume that the number of moving particles is distributed according to a negative binomial distribution (11), whose parameters are given by Equation 12. We also assume that the instantaneous particle velocity $u_{p,i}$ is normally distributed (see Equation 5). We assume that the two marginal probabilities P_n and P_u fully describe the process or, to put it differently, there is no correlation between N and $u_{p,i}$. We define U as the sum of the particle velocities:

$$U = \sum_i^N u_{p,i}. \tag{19}$$

As the volume-averaged particle transport rate in the control window $\mathscr{V}$ is $q_s = U/L$, the probability density function of q_s is related to that of U:

$$P_{q_s} = L P_U(L q_s). \tag{20}$$

The probability P_U of U is obtained by summing the elementary probabilities of observing k particles, in the control window, whose velocity sum equals U:

$$P_U = \sum_{k=1}^{\infty} P_n(k) P_k(U), \tag{21}$$

where P_k denotes the probability of observing that the velocity sum is equal to U. As the sum of normally distributed random variables is also normally distributed, P_k is the normal distribution $\mathscr{N}$, with mean $k\overline{u}_p$ and standard deviation $\sqrt{k}\sigma_u$. We then deduce

$$
\begin{aligned}
P_{q_s} = L P_U(L q_s) &= L \sum_{k=1}^{\infty} P_n(k) P_k(L q_s) \\
&= \sum_{k=1}^{\infty} L \binom{q+n-1}{q-1} p^q (1-p)^n \mathscr{N}(k\overline{u}_p/L, \ \sqrt{k}\sigma_u/L)(L q_s).
\end{aligned}
\tag{22}
$$

It is then straightforward to infer the mean and variance of q_s even though there is no closed-form expression for the probability P_{q_s}:

$$\langle q_s \rangle = \int_{\mathbb{R}} q_s P_{q_s} \mathrm{d}q_s = \frac{N_{ss}}{L} \bar{u}_p, \tag{23}$$

$$\mathrm{var}\, q_s = \int_{\mathbb{R}} (q_s - \langle q_s \rangle)^2 P_{q_s} \mathrm{d}q_s = \mathrm{var}_{ss} N \frac{\bar{u}_p^2 + p\sigma_u^2}{L^2}. \tag{24}$$

When $\sigma_u = 0$, we retrieve the variance given by Equation 18. In Appendix C, we show that if we select an exponential distribution for the particle velocities, then there is no change in the ensemble average and only a slight change in the ensemble variance.

If we assume that events (particle velocity and particle number) are independent, then we can generalize the variance Equation 18 to take velocity fluctuations into account in the double-averaged variance by following the same reasoning as that used for deriving Equation 18:

$$\mathrm{var}\, \overline{q}_s(\Delta t|t) = \frac{\bar{u}_p^2 + p\, \mathrm{var}\, u (\lambda + \nu_{\mathrm{in}})(\nu_{\mathrm{out}} + \sigma)}{L^2 \Delta t \quad (\nu_{\mathrm{out}} + \sigma - \mu)^3} = \mathrm{var}_{ss}\, N \frac{\bar{u}_p^2 + p\, \mathrm{var}\, u}{L^2} \frac{t_c}{\Delta t}. \tag{25}$$

2.6. Summary of Results

When we considered that a steady-state system in which the particle flux across a vertical control surface $\mathscr{S}$ was a Poisson process with rate Λ, we found that the double-averaged particle flux (8) was Λ, independently of the sampling duration Δt. Under steady-state conditions, mass conservation imposes that $\nu_{\mathrm{in}} = \nu_{\mathrm{out}} \langle N \rangle_{ss}$ in the control window $\mathscr{V}$. Using Equation 10, we then deduced that the double-averaged bedload transport rate (15) or (23) was also Λ in the limit $\Delta t \gg t_c$. We thus concluded that, on average, both transport rate definitions provided identical results:

$$\langle \overline{q}_s \rangle = \langle \overline{\Phi}_s \rangle. \tag{26}$$

These results, however, differed with regard to the variance of q_s or Φ_s: the variance of the double-averaged flux $\langle \overline{\Phi}_s \rangle$ varied as $\Lambda/\Delta t$, whereas the variance of the double-averaged transport rate $\langle \overline{q}_s \rangle$ varied like $\nu_{\mathrm{out}}^2 \mathrm{var}\, s_s N t_c/\Delta t$ given by Equation 18 (or like Equation 25 if velocity fluctuations were taken into account). The fact that the variance varied like $1/\Delta t$ comes as no surprise because the central limit theorem states that the scaled sum S_n of n *independent and identically distributed random* variables Y_i (with finite mean μ_y and standard deviation σ_y) converges in distribution to a normal distribution with mean 0 and variance 1 (Grimmett & Stirzaker, 2008):

$$\frac{S_n - n\mu_y}{\sqrt{n}\sigma_y} \xrightarrow{d} \mathscr{N}(0, 1). \tag{27}$$

If we apply the central limit theorem to a long time series $(t_i = i\delta t, y_i)$, where $1 \leq i \leq n$ and where δt denotes the time interval between two measurements, with $y_i = \mathscr{Q}_i$ the transport rate at time t_i, then the time-averaged bedload transport rate is $\overline{q}_s(t_n) = S_n \delta t/\Delta t$. Furthermore, when n is large, we have: $\overline{S}_n \to n\mu_y$ and $\mathrm{var}\, S_n \to n\sigma_y^2$, thus $\overline{\mathscr{Q}}_s \to \mu_y$ and $\mathrm{var}\, \mathscr{Q}_s \to \sigma_y^2 \delta t/\Delta t$ because $n \propto \Delta t/\delta t$. Asymptotically, for any sample that satisfies the application conditions of the central limit theorem, then the relation $\mathrm{var}\, \overline{q}_s \propto \Delta t^{-1}$ also holds true. The difference between this scaling and Equations 18 and 9 is that in the Markovian case, the variation $\mathrm{var}\, \overline{q}_s \propto \Delta t^{-1}$ holds exactly for any sampling duration Δt. Furthermore, in the case of a Poisson process, the steady-state variance in Equation 9 is entirely controlled by the mean particle flux Λ, and there is no need to introduce another parameter σ_y to find its value.

2.7. Protocol for Measuring the Sediment Transport Rate and Its Variance

In Equations 8 and 15, the transport rates $\langle \overline{\Phi}_s \rangle$ and $\langle \overline{q}_s \rangle$ are based on ensemble averages. The problem is that it is difficult to calculate ensemble averages directly in experiments (unless many runs of the same experiment can be made). There is, however, a fairly simple technique that mimics the ensemble average and makes it possible to deduce the sample mean and variance with high precision: the *bootstrap method* (Davison & Hinkley, 1997). Like the jackknife, this is a resampling technique, which involves repeatedly drawing random subsamples from a single original sample and generating new samples with similar
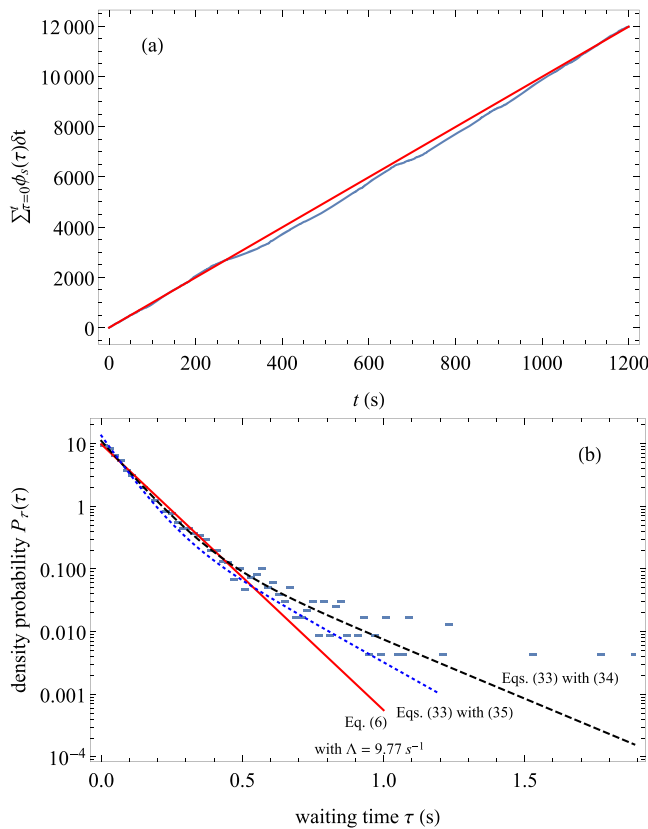
Figure 4. (a) Variation over time of the cumulative number of particles crossing the control surface $\sum_0^t \varphi_s(\tau)\delta t$. The red line represents the cumulative number of particles $\sum \varphi_s \delta t = \hat{\Lambda} t$ with $\hat{\Lambda} = \nu_{\text{in}} = 9.98$ grains/s. (b) Waiting times for the flux at the control window's downstream end $\mathcal{S}$. The solid red line represents the exponential distribution (6) with rate $\tilde{\Lambda} = 9.77 \text{ s}^{-1}$ adjusted on the waiting time sample using the method of moments. The dashed black line represents the hyperexponential distribution (33) fitted to the data using the method of moments. The dotted blue line represents the hyperexponential distribution (35) adjusted on the flume inlet's data. The light blue dots show the empirical probabilities.

statistical properties to those exhibited by the original one (Davison & Hinkley, 1997). We assume a time series $(t_i = i\delta t, y_i)$ $(1 \le i \le n)$, where the variables y_i are independent and identically distributed random values drawn from an underlying distribution F. We assume that we do not know F, but we can get an empirical estimate $\hat{F}$ by using the sample $(y_1, y_2, \ldots, y_n)$. We can then draw M samples of n values from $\hat{F}$. We use these M samples to compute the sample mean and variance.

Thus, the key point is starting with a sample of independent and identically distributed data. The tests are detailed in section 4. Here, we would like to highlight a simple test of stationarity, which turns out to be robust and useful in a variety of settings. Because of the existence of fluctuations in the q_s time series, it may be difficult to distinguish between stationarity, weak stationarity, and absence of stationarity. Below, we plot the cumulative amount of sediment $S_n = \sum_{i=1}^n y_i \Delta t$ (here y_i denotes the particle flux Φ_s or volume-averaged transport rate q_s) as a function of time (see Figure 4 for an example). If the steps (t_n, S_n) come close to a straight line of slope $\hat{\Lambda}$, then the process is probably stationary: The mean flux will be close to $\hat{\Lambda}$. Should only some groups of intervals (t_n, S_n) form segments of the line, then the process is weakly stationary. These groups can then be used to identify the periods during which the process was reasonably close to a stationary process. If there is no good match between these groups and the line representing steady state, the protocol cannot be applied.

Our protocol for defining the mean bedload transport rate and its variance is the following:

- If we can acquire data at a sufficiently high frequency, then we resolve the times at which particles cross the control surface $\mathcal{S}$ or move within the control window $\mathcal{V}$. We can then determine the waiting time between particle arrivals or measure particle velocity. This is the ideal case against which we will test the theory outlined in this section. Although an emphasis is placed on Markovian processes, particles may behave differently; notably, many particles cross the control surface $\mathcal{S}$ within a short time-interval ("many" here means that the number of particles crossing the surface cannot be described using the Poisson law). Appendix B shows how renewal theory can be used in these cases.
- In the opposite case, when the data acquisition rate is low (typically below 1 Hz), we can still apply the protocol, but it will be difficult to verify whether the theory described above captures the flux behavior well. The central limit theorem is, however, sufficient to deduce the key information of the bedload transport rate's mean and variance. There is, of course, no free lunch. The price paid for low-frequency measurements is that the fluctuation strength is independent of the mean particle flux. Naturally, this does not cause trouble when working under steady-state conditions (one can estimate σ_y), but it becomes more problematic under time-dependent flow conditions.

The steps are the following:

1. Plot the cumulated amount of sediment on a graph $(t_n, S_n = \delta t \sum_{i=1}^n y_i)$ and identify the periods T during which the steps are close to a straight line of slope $\hat{\Lambda}$, that is, the period during which the process was stationary or quasi-stationary. The slope $\hat{\Lambda}$ represents the mean transport rate over time T, and S_n is a time discretization of $\int y(t)dt$.
2. From this period T, we can extract a sample (t_i, y_i) involving $n_T \sim T/\delta t$ values. Because we need to handle independent and identically distributed random variables y_i, we must check that this assumption is satisfied. In practice, if one measures volume-averaged transport rates q_i, the assumption of independent and identically distributed data implies that the time interval δt should be larger than the autocorrelation

time, otherwise neighboring values would be correlated. The "training" sample $(t_i, y_i)_{1 \leq i \leq n_T}$ is used to generate random samples, using the bootstrap resampling technique (Davison & Hinkley, 1997).

3. We can estimate the variance of $\langle \bar{y} \rangle (\Delta t)$ by generating M samples (typically $M = 100$ is recommended) of size $n_r = \Delta t / \delta t$ from the training sample (e.g., see Davison & Hinkley, 1997) on how to use the bootstrap method) and estimating the variance var $\hat{y}$ of this group.

4. When plotted as a function of Δt, the empirical variance var $\hat{y}$ should lie on the curve $\hat{\Lambda} / \Delta t$, by virtue of Equation 18 or 9, if the data were collected at a sufficiently high frequency. If they were not, we can use the central limit theorem (27), and the data should be close to the curve $\sigma_y \delta t / \Delta t$.

5. The empirical variance curve var $\hat{y}(\Delta t)$ makes it possible to specify the accuracy associated with the measurement of the double-averaged transport rate over the duration Δt or, reciprocally, to select the value of Δt that corresponds to the desired accuracy (i.e., the prescribed σ_y).

3. Experimental Procedure

3.1. Experimental Setup

The flume used was 2.5 m long, 40 mm wide, and tilted at an angle of 1.55° from the horizontal. Water discharge at the flume inlet was set to $Q_w = 0.2$ L/s, and flow depth was 1.1 cm (the hydraulic radius was $R_h = 71$ mm). The flow was supercritical (with a Froude number of 1.1). This choice of the flow regime was driven by our desire to approach the flow conditions found in mountain streams (the subject of our research) and to limit the effects of sidewall friction on flow turbulence. Well-sorted gravel (mean diameter $d_{50} = 3$ mm, density $\varrho_p = 2,550$ kg/m^3) was layered along the flume bottom to a thickness of 4 cm, and the same gravel was used to feed the flume at a feed rate of 10.3 ± 0.5 grains/s. The Shields number was $\Theta = \varrho_h / ((\varrho_p - \varrho) d_{50}) = 0.043$ (if we use the empirical equation for gravel beds proposed by Recking (2013), we obtain $\Theta = 0.045$). We designed a specific system to feed the flume with sediment (see supportinginformation for photographs), bounded by two constraints: The feed rate had to be low (a few grains per second), and the particle flux had to be as close to a Poisson process as possible. Gravel was initially contained in a hopper whose opening controlled the inflow rate. The particles fell onto a slowly rotating cylinder ($\Omega = 0.4$ rad/s) whose surface was covered with sandpaper. A vertical brush prevented grains from stacking and generating avalanches. After the cylinder had rotated by a certain angle, any grain stuck to the rough cylinder exterior was dislodged and fell into the flume. The grains fell onto a smooth white board, slipped down it while being filmed by a high-speed camera, and then arrived at the flume inlet, where they were entrained by the flow. Although the match was not perfect, the particle flux at the flume inlet was very close to a Poisson process.

3.2. Image Processing and Tracking

Images were collected at 250 frames per second using a high-speed Basler A504k camera equipped with a Nikkor-S 1:1.4 $f = 50$ mm lens, at a resolution of 624×300 pixels (with the scale 1 px $=$ 0.133 mm). A 35-cm-long transparent plastic plate was placed above the water surface to prevent reflections and image distortion created by free surface waves. Images were taken from vertically above this plate. This setup caused a local flow disturbance whose effects were negligible on the flow portion under the plate, although we presume that it exacerbated bedforms downstream of the plate. Three LED spotlights illuminated the control window homogeneously. The experimental run lasted 22 min, and initial images were removed to extract a sequence of 20 min.

The raw images were processed by subtracting their background image, defined as the median of the 20 previous frames. This preliminary step enabled us to highlight moving particles and discard jiggling particles which were not being transported by the flow. Particle tracking was based on a procedure available from the TrackMate-ImageJ numerical framework (Tinevez et al., 2017). First, spot detection was carried out using a Laplacian of the Gaussian detector and considering an estimate of the mean grain size in the images as the detector size parameter. Second, in the particle linking step, we modified and used the Linear Assignment Problem (LAP) tracker initially proposed by Jaqaman et al. (2008): we modified the linking cost function so that it accounted for the preferential direction of particle displacement (downstream in our case). The *gap closing* option was allowed over two time steps. Moreover, spots and trajectories were filtered to reduce tracking errors, mostly caused by moving bubbles trapped at the interface between the transparent plate and the water flow. After the spot detection step, we filtered spots by considering their properties,

which enabled us to identify spots associated with moving bubbles. We rejected spots characterized by an estimated diameter smaller than 7 px and/or by a maximum pixel intensity higher than 160 (over 255). Among the trajectories reconstructed using the particle linking procedure, we discarded those composed of fewer than four spots in order to remove short tracklets caused by bubbles and improper particle linking. A validation test of this tracking method was conducted, and it is presented in the supporting information.

Finally, the resulting tracks were analyzed to calculate the variables of interest for the present study: We emphasized the time series $(t_i, N(t_i))$ of the number of moving particles, the distribution of the particle velocity u_p (averaged over all particle paths for each image), and the time series of the particle fluxes in the downstream section of the control window $\Phi_s(t)$. We considered three control windows of different streamwise lengths ($L = 17.5$, 35, and 70 mm), all located in the same section and starting 1.32 m from the flume inlet ($x = 0$). We present only results obtained with the longest window $L = 70$ mm. See the supporting information for further data on L's influence on the results (which was found to be small, on average).

4. Results

This section addresses the following points. First, we compare the various predictions of the Markovian theory developed in section 2 against high-resolution experimental data. Second, we test the protocol proposed in section 2.7. Third, to estimate whether this protocol has potential, we evaluate its performance under more complicated flow conditions: Because bedforms developed downstream of the plate and thus influenced the bedload transport rate, we look more closely at the data acquired at the flume outlet. Before addressing each of these points, we adjust the model parameters $\lambda, \mu, \sigma, \mu, \nu_{out}, \bar{u}_p$, and σ_u from the time series $(t_i = i\delta t, N_i, u_i)$, where $\delta t = 4$ ms is the time interval between two images, and N_i is the number of moving particles in the control volume. The inflow rate $\nu_{in} = 10.3$ grains/s was imposed experimentally at the flume inlet.

4.1. Parameter Estimation

Of five model parameters—entrainment parameters (λ and μ), deposition rate (σ), flux parameters (ν_{out}, and ν_{in})—four are unknown and $\nu_{in} = 9.98$ grains/s was set experimentally (taking the value measured in the control window rather than the one fixed at the flume inlet). We only need to select four relationships to determine the unknowns, but at least five equations are available:

1. Bed equilibrium

$$\sigma \langle N \rangle_{ss} = \mu \langle N \rangle_{ss} + \lambda. \tag{28}$$

2. Flux steadiness

$$\nu_{in} = \nu_{out} \langle N \rangle_{ss}. \tag{29}$$

3. Condition on the average N value

$$\langle N \rangle_{ss} = \frac{\beta}{\alpha} = \frac{\lambda + \nu_{in}}{\nu_{out} + \sigma - \mu}. \tag{30}$$

4. Condition on the N variance

$$\text{var}_{ss} N = \frac{(\lambda + \nu_{in})(\nu_{out} + \sigma)}{(\nu_{out} + \sigma - \mu)^2}. \tag{31}$$

5. Condition on the autocorrelation time

$$\nu_{out} + \sigma - \mu = t_c^{-1}. \tag{32}$$

Table 1
Empirical and Theoretical Probabilities of Observing k Particles Crossing the Control Surface $\mathcal{S}$ Within the Time Interval $\delta t = 4\ ms$

k	Empirical value	Poisson prediction	Relative error
$k = 0$	0.959587	0.959567	0.002%
$k = 1$	0.039559	0.039604	−0.112%
$k = 2$	8.4×10^{-4}	0.00081	3.59%
$k = 3$	6.7×10^{-6}	11.1×10^{-6}	−40.71%

The autocorrelation time was $t_c = 221$ ms (see Figure 6b). We set ν_{out} from Equation 29: $\nu_{\text{out}} = \nu_{\text{in}}/\langle N \rangle_{\text{ss}} = 1.88$ 1/s. We solved Equations 30, 31, and 32 for λ, μ and σ. We found $\lambda = 14.77$ grains/s, $\mu = 4.98$ 1/s, and $\sigma = 7.68$ 1/s. Furthermore, we inferred from the processed images that the mean particle velocity was $\bar{u}_p = 13.41$ cm/s and its standard deviation was $\sigma_u = 3.24$ cm/s. Note the value $\nu_{\text{out}} = 1.82$ 1/s was 5% below the theoretical value $\nu_{\text{out}} = \bar{u}_p/L = 1.91$ 1/s. Equation 28 was used to test whether the fitted values were consistent with the assumption of bed equilibrium.

4.2. Particle Flux

We begin our analysis with the particle flux across the control surface $\mathcal{S}$ located at the control volume's downstream end. Grains crossed the control surface at a mean rate $\hat{\Lambda} = N_{\text{tot}}/T_{\text{exp}} = \nu_{\text{in}} = 9.98$ grains/s ($N_{\text{tot}} = 11{,}974$ was the total number of grains to have crossed $\mathcal{S}$ over the run duration $T_{\text{exp}} = 1{,}200$ s). As shown by Figure 4a, the particle flux was almost stationary, even though the time variations in Φ_s exhibited wide fluctuations over short time scales (see Figure 8). The mean number of particles crossing the control surface $\mathcal{S}$ within $\delta t = 4$ ms was $\overline{N} = 0.04127$, whereas the variance was var $N = 0.04130$. The 0.07% deviation between these two values shows that the assumption of a Poisson process was realistic. Table 1 shows that the Poisson model properly predicts the number of particles crossing the window per time interval δt. The error for $k = 3$ particles is likely to have resulted from the sample's finite size (only three occurrences in 1,200 s). The partial autocorrelation function was close to 1 for a lag of 1, then vanishingly small for lags larger than 1, as expected for a Poisson process.

Stationary jump processes are fully characterized by the probability of observing the process in a given state and by the waiting times τ between two jumps (Gillespie, 1992). Although Table 1 and Figure 4a support the idea of a Poisson process, examining the waiting-time distribution tells us a different story: Figure 4b shows the empirical probability density function of waiting times and their exponential distribution (6) (with rate $\widetilde{\Lambda} = 9.77\ \text{s}^{-1}$ adjusted on the waiting time sample using the method of moments). Over short periods, there was a fairly good match between the empirical and theoretical distributions, but for periods longer than 400 ms, deviation from the exponential distribution was marked. The sample's coefficient of variation was $\sigma_\tau/\overline{\tau} = 1.21$ (standard deviation $\sigma_\tau = \sqrt{\text{var}\ \tau} = 124$ ms, mean $\overline{\tau} = 102$ ms), thus higher than unity. This confirmed that waiting times were not strictly exponentially distributed. To better describe the probability distribution of waiting times, we can adjust a two-parameter hyperexponential distribution, whose density function is

$$p(\tau) = \alpha_1 \lambda_1 \exp(-\lambda_1 \tau) + \alpha_2 \lambda_2 \exp(-\lambda_2 \tau), \tag{33}$$

where α_1 and α_2 are mixture parameters satisfying $\alpha_1 + \alpha_2 = 1$, whereas λ_1 and λ_2 are two rates. Using the method of maximum likelihood, we found

$$\alpha_1 = 0.13, \quad \lambda_1 = 4.33 \quad \text{s}^{-1}, \quad \alpha_2 = 0.87, \quad \text{and} \quad \lambda_2 = 12.04 \quad \text{s}^{-1}, \tag{34}$$

which was associated with slightly (20%) higher rates than those fitted at the flume inlet:

$$\alpha_1 = 0.19, \quad \lambda_1 = 5.8 \quad \text{s}^{-1}, \quad \alpha_2 = 0.81, \quad \text{and} \quad \lambda_2 = 15.2 \quad \text{s}^{-1}. \tag{35}$$

To compute the sample mean and variance for the time series (t_i, n_i), we used the bootstrap method and generated $M = 100$ samples from the experimental data set (see section 2.7). If the process was stationary and Poissonian with rate Λ, then we would expect that

$$\langle \overline{\Phi}_s \rangle \rightarrow \Lambda \quad \text{and} \quad \text{var}\ \overline{\Phi}_s(\Delta t) \rightarrow \frac{\Lambda}{\Delta t}, \tag{36}$$

as seen in section 2.3. The parameter Λ was estimated by fitting an exponential distribution to the waiting times between two positive jumps (i.e., events for which $n_i > 0$) in the time series (t_i, n_i). We found $\tilde{\Lambda} = 9.77$ s^{-1}. Note the slight difference (2%) in the mean transport rate calculated using the assumption of a Poisson process ($\overline{\Phi}_{\text{ss}} = \Lambda = 9.77$ grains/s) and the one obtained empirically by setting $\overline{\Phi}_{\text{ss}} = \hat{\Lambda} = N_{\text{tot}}/T_{\text{exp}} = 9.98$
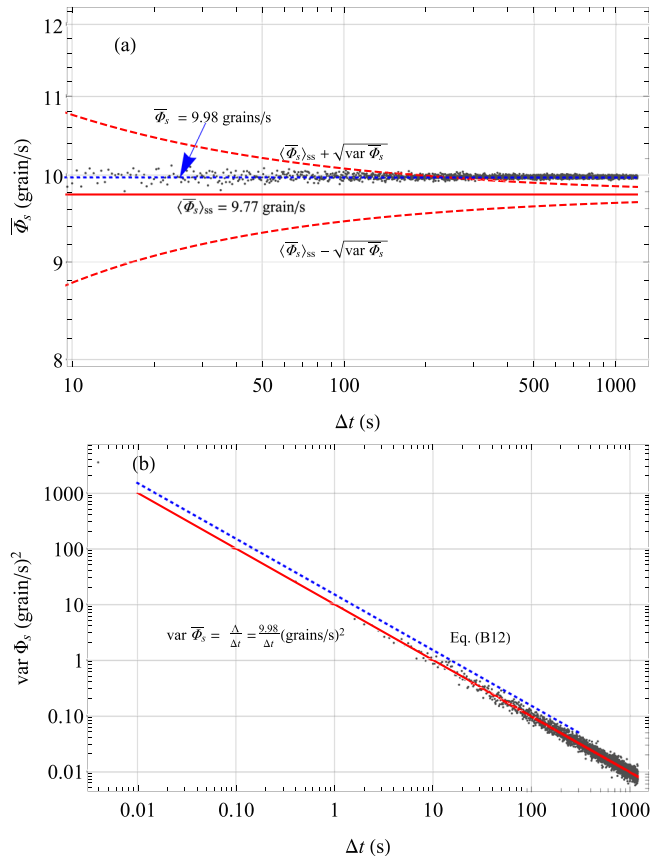
Figure 5. (a) Influence of sampling duration on the computation of the sample mean. The solid red line is the theoretical mean value given by Equation 36, while the dashed red lines show the uncertainty domain $\langle \Phi_s \rangle_{ss} \pm \mathrm{var}\, \Phi_{ss}$. The dotted blue line is the empirical mean flux $\Phi_{ss} = \hat{\Lambda} = N_{tot}/T_{exp} = 11,974/1,200 = 9.98$ grains/s. (b) Influence of sampling duration on the sample variance. For both plots, the blue dots were obtained using the bootstrap method. The solid red line shows the theoretical variance (9) with $\Lambda = \hat{\Lambda} = 9.98$ grains/s, whereas the dashed blue curve shows the variance (B12) derived from the renewal model.

grains/s. As shown in Figure 4b, the process was not a genuine Poisson process, and this led to small errors. This explains why the empirical means computed using the bootstrap method were close to the mean flux value $\overline{\Phi}_{ss} = \hat{\Lambda} = 9.98$ grains/s (see Figure 5a), and 2% higher than the rate $\widetilde{\Lambda}$ deduced from the waiting-time distribution. For the variance $\mathrm{var}\, \Phi_s(\Delta t)$, Figure 5b shows the excellent agreement between the variances computed using the bootstrap method and the theoretical prediction (36).

We also used renewal theory for computing the particle flux (see Appendix B). Here, we used the hyperexponential distribution to estimate the waiting time between two events. The number of particles which could arrive at the same time was estimated using the binomial-like distribution (B1). From the experimental data, we deduced that there was a probability of $p = 11,473/11,989 = 0.979$ that a single particle crossed $\mathcal{S}$ within δt, and of $1-p$ that two particles crossed it at the same time. This resulted in a flux average (B11) that closely matched the feed rate $\hat{\Lambda} = 9.98$ grains/s, as shown in Figure 5a. This confirmed that the slight discrepancy between theory and experiment was likely due to the existence of much longer waiting times than predicted by the exponential distribution. For the variance, our renewal model provided only the asymptotic scaling (B12): $\mathrm{var}\, \Phi_s \approx 15.2/\Delta t$ grains^2/s^2, which resulted in the right trend (var $\Phi_s \propto (\Delta t)^{-1}$, but overpredicted variance by 50%. This may seem surprising—because the renewal model performed better than the Markovian model at predicting the sample mean in Figure 5a—but it should be remembered that Equation B12 is an asymptotic expression that holds for sufficiently long times Δt. Further simulations (not shown here) of the renewal process, presented in Appendix B, confirmed the sample variance's sensitivity to sample size.

4.3. Volume-Averaged Transport Rate

We recorded the number N of moving particles in each frame. The time-averaged number of moving particles was $\overline{N} = 5.47$, whereas the variance was $\mathrm{var}\, N = 11.5$. Figure 6a shows that the negative binomial model closely matched the statistical distribution of the number of particles moving in the window during time interval δt. The error was usually less than 6%, except at $n = 0$ where it reached 30%. The time series shows large fluctuations in N, with peaks as large as $5\overline{N}$. Figure 6b shows that the exponential autocorrelation function (13) fitted the empirical autocorrelation function if we set $t_c = 221$ ms. The particles moved at a mean velocity $\bar{u}_p = 13.45$ cm/s (standard deviation $\sigma_u = 3.76$ cm/s). The Gauss-Laplace distribution offered a rough description of particle velocity fluctuations (see Figure 6d). The stationarity test confirmed that the (t_i, q_i) was a stationary process, with a mean rate $\hat{q}_{ss} = 10.27$ grains/s.

We used the bootstrap method to evaluate how the sample mean $\langle \overline{q}_s \rangle$ and variance $\mathrm{var}\, \overline{q}_s$ were dependent on sampling duration Δt. As the autocorrelation time $t_c = 221$ ms was fairly long compared to the acquisition time $\delta t = 4$ ms ($t_c/\delta t \sim 50$), we had to resample the raw data series (t_i, N_i) at a frequency of $1/(50\delta t) = 5$ Hz to obtain a sample of independent and identically distributed data. Figure 7a shows that the mean computed using the bootstrap method was close to 10.25 grains/s, a slightly (2%) higher value than the time-averaged flux $\langle \overline{\Phi}_s \rangle_{ss} = 9.98$ grains/s. Figure 7b shows the excellent agreement between the sample variances and their theoretical prediction (18). Because the velocity fluctuations here were small compared to their mean, taking velocity fluctuations into account did not lead to better results. This confirmed the observation, made by a number of authors (Ancey et al., 2008; Campagnol et al., 2012; Cudden & Hoey, 2003; Singh et al., 2009), that
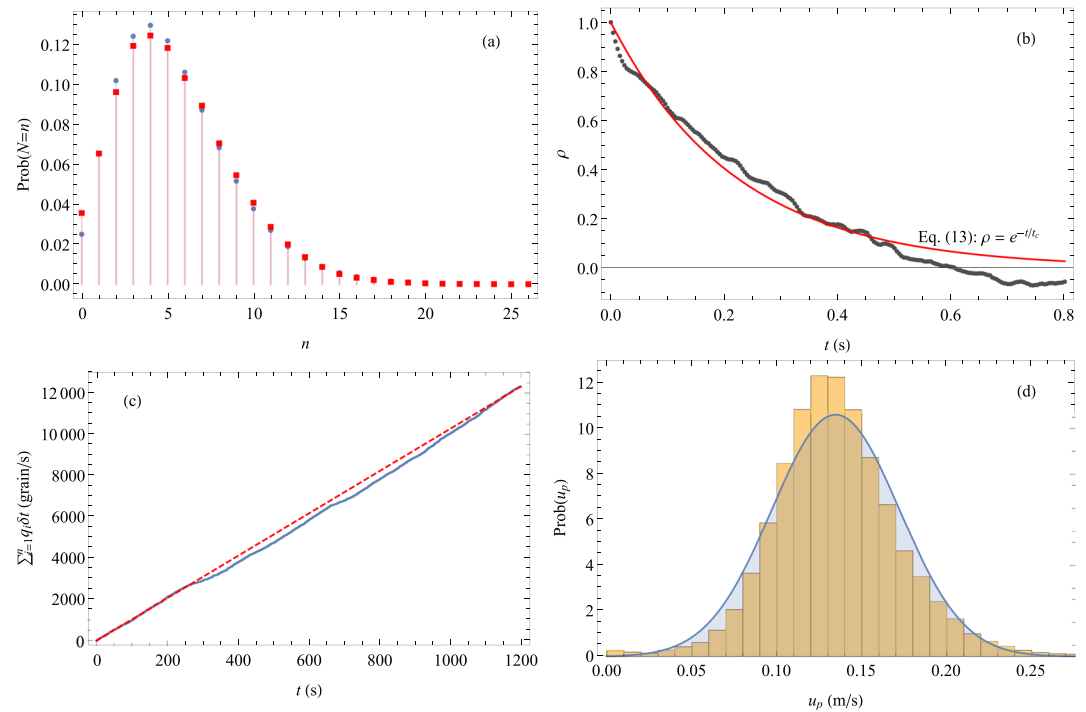
Figure 6. (a) Comparison between the empirical (blue dots) and theoretical (red squares) negative binomial probability densities (11). (b) Autocorrelation function of $N(t)$: the black dots are the empirical function, and the solid red line shows the theoretical exponential function (13) with $t_c = 221$ ms. (c) Stationarity tests on the (t_i, q_i) time series: The solid line shows $\sum_i q_i \delta t$, whereas the dashed line is the cumulative mass $\hat{q}_{ss} t$ with $\hat{q}_{ss} = 10.27$ grains/s the bedload transport rate averaged over the run duration. (d) Particle velocity distribution: In addition to the histogram, we have plotted the Gauss–Laplace distribution (5) fitted to the data (solid blue line).

bedload transport fluctuations originate primarily from variations in the number of moving particles rather than from their velocities.

4.4. Influence of the Sampling Duration on the Time Series

When comparing the means and variances of the particle flux (section 4.2) and volume-averaged transport rate (section 4.3), we found that the two definitions led to similar values (to within a few percent) and the same dependence on the sampling duration Δt. Although this finding made sense intuitively, it was not easy to anticipate it from the theoretical results in section 2.

This similarity holds only on average. As shown by Figure 8, time series aspects depend a great deal on the definition of q_s and the sampling duration. Using short sampling durations, the particle flux showed wide fluctuations as there was no time correlation between the two measurements. On the contrary, the bedload transport rates were correlated because the acquisition frequency was much higher than $1/t_c \sim 5$ Hz. Using longer sampling durations (typically for $\Delta t \geq 1$ s), the two time-averaged time series look generally similar. For $\Delta t = 1$ s, instantaneous differences $\epsilon = \overline{q}_s / \overline{\Phi}_s - 1$ exceeding 100% were observed (see Figure 8b), and, on average, the mean difference $\overline{\epsilon}$ reached 7%. For $\Delta t = 10$ s, the relative differences were usually less than 20%, whereas the mean difference between the two time series dropped below 3%.

4.5. The Influence of Bedforms

Bedforms developed along the bed downstream of the observation plate covering the free surface. Forms were likely exacerbated by the plate as we observed a clear difference in behavior upstream and downstream of it:

- Downstream of the plate, we observed upstream-migrating antidunes. Their wavelength ranged from ≈8 to 15 cm, and their amplitude was close to $2d_{50}$. Their celerity was in the 1–1.5-mm/s range, but they moved intermittently.
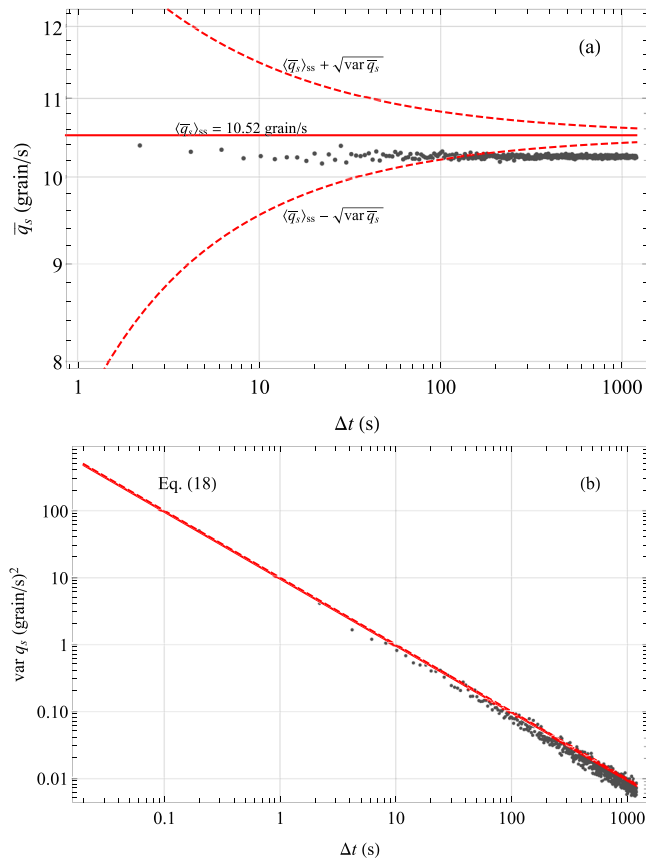
Figure 7. (a) Influence of the sampling duration Δt on the computation of the sample mean: The black dots show the values generated using the bootstrap method. The solid red line shows the theoretical value (15). (b) Influence of the sampling duration on the computation of the sample variance. The solid red line shows the theoretical prediction (18) when assuming $\sigma_u = 0$ (i.e., velocity fluctuations are negligible), whereas the dashed red curve shows the theoretical prediction (25) when $\sigma_u > 0$. The latter curve is hardly discernable from the former as $\sigma_u \sim 0.07 \bar{u}_p^2$.

- Upstream of the plate, behavior was more complicated. Bed undulations were observed, but their origin and nature remained uncertain (perhaps they were sediment waves). Their wavelength fluctuated widely from 4 to 8 cm, and their amplitude was approximately one grain diameter. These forms experienced cycles of growth and decay over time scales of a few minutes, with no evidence of migration (see Movie S2).

We also measured an 11% increase in the bedload transport rate: Over 20 min, a total of 13,271 particles left the flume, whereas 11,974 crossed the control surface $\mathcal{S}$ located in the middle of the flume. The Φ_s time series was more intermittent: Pulses of intense activity were separated by periods of lower activity, which was also reflected in longer waiting times between particle arrivals (waiting times as long as 6 s were measured) as shown by Figure 9a. Examining time variations in the cumulative amount of sediment shows that during the first 6 min, the particle flux was much higher than the feed rate (16.3 grains/s versus 10.3 grains/s, on average, at the flume inlet) (see Figure 9b). After a phase that lasted about 100 s (between $t = 340$ and 440 s) and during which the mean particle flux dropped to 2.7 grains/s, there was a period $440 \leq t \leq 1{,}080$ s during which the particle flux remained almost constant ($\overline{\Phi}_s = 10.2$ grains/s) and close to the feed rate. We thus extracted a reduced sample between the timepoints $440 \leq t \leq 1{,}080$ s.

Figure 9c shows that the double-averaged means (estimated using the bootstrap method) tended toward the mean particle flux $\hat{\Lambda}_r = N_r/640 = 10.77$ grains/s obtained by dividing the number of particles $N_r = 6{,}896$ leaving the flume between time points $t = 440$ and $t = 1{,}080$ s, by the length of time $1{,}080 - 440 = 640$ s. As expected, the bootstrap method provided a correct estimate of the mean particle flux for this period. As the waiting-time distribution deviated from the exponential distribution, the particle rate deduced from the mean waiting time, $\widetilde{\Lambda}_r = 9.87$ grains/s, underestimated the actual transport rate by 8%. Applying the renewal model (B11) led to a mean transport rate $\overline{\Phi}_s = 10.66$ grains/s, which was 1% below the actual rate. The main effect of bedforms was thus to alter the temporal distribution in the number of particles: the temporal distribution deviated gradually from the Poisson distribution as a result of increased intermittency, that is, alternating between periods during which no transport occurred and periods during which more intense sediment transport took place. Figure 9d shows that the double-averaged variance varied as $\hat{\Lambda}_r/\Delta t$, as expected.

The forms observed upstream of the plate were likely driven by alternate phases of sediment storage (over periods spanning tens of seconds) and fast release of particle clusters. It is probable that this alternation changed the waiting-time distribution in the control window and created the hyperexponential tail shown in Figure 4b. Downstream of the plate, the antidune migration period (in the 80–150-s range) was consistent with the time intervals between the bedload flux pulses recorded at the flume outlet (Figure 1). We believed that the hyperexponential waitingtime distribution at the flume outlet (Figure 9) was due to antidune migration.

5. Applications

We finish the paper by describing two potential applications for the measurement protocol outlined in section 2.7:

- We ran long-duration experiments under steady-state conditions in a laboratory flume (see section 5.1). As gravel bars and pools developed and migrated along the flume bed, the bedload transport measured
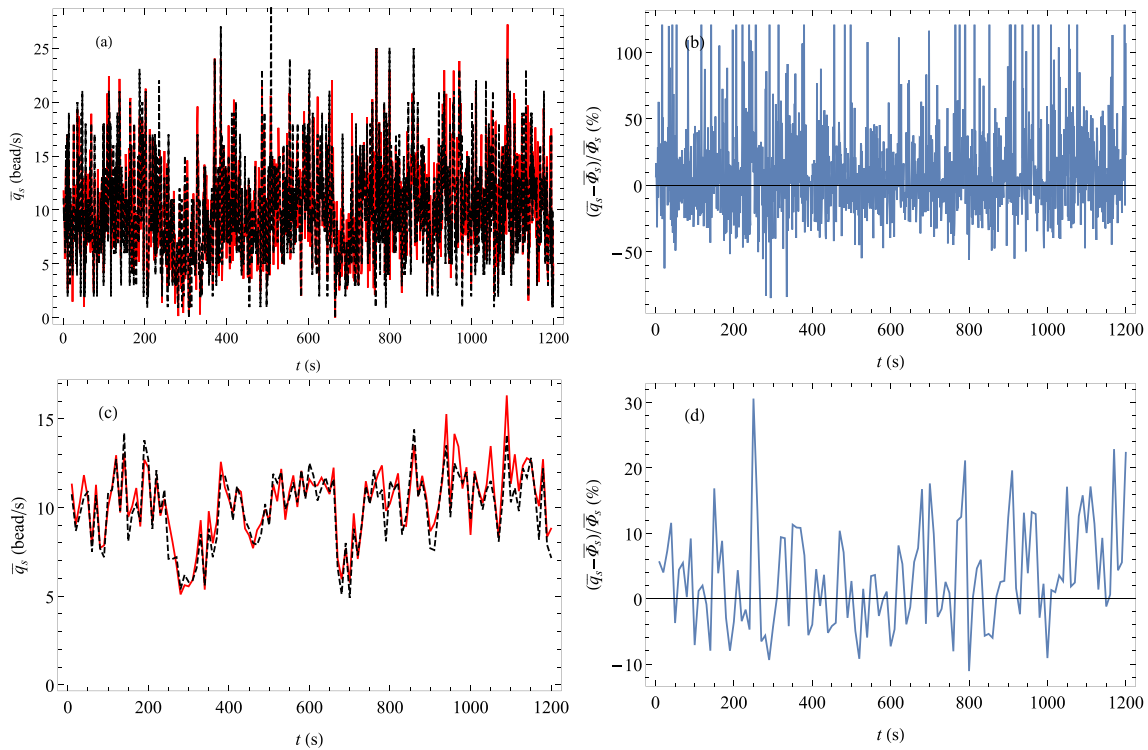
Figure 8. (a) Time variations in the time-averaged transport rate q_s (solid red line) and particle flux (dashed black line) Φ_s for a sampling duration $\Delta t = 250\delta t = 1$ s. (b) Relative difference between q_s and Φ_s as a function of time t for $\Delta t = 1$ s. (c) Time variations in the time-averaged transport rate q_s(solid red line) and particle flux (dashed black line) Φ_s for a sampling duration $\Delta t = 2500\delta t = 10$ s. Relative difference between q_s and Φ_s as a function of time for $\Delta t = 10$ s.

at the flume outlet exhibited wide fluctuations resulting from alternating phases of low and intense transport. Bedload transport pulses were often associated with the destruction of bars, which released large amounts of gravel (Dhont & Ancey, 2018).

• We have been monitoring a gravel-bed river in the Swiss Alps since 2011 (see section 5.2). Contrary to other applications in this paper, this was not a steady-state system, but there were periods during which it approached a steady state, which made it possible to apply our measurement protocol.

These two applications illustrate the sampling duration's significance to the estimation of bedload transport rates. To obtain fairly high precision (10% variance or lower), one has to carefully study how the Q_s variance changes with the sampling duration Δt.

5.1. Laboratory Flume

Here, we show how the measurement protocol performed with a time series of bedload transport rates measured at the outlet of a flume 19 m long, 60 cm wide, and inclined at 1.6% to the horizontal. We used gravel whose median diameter was $d_{50} = 5.5$ mm. The water discharge was constant $Q_w = 15$ L/s. Transport rates were measured using impact plates and accelerometers operated at 100 Hz for a long period ($T_{\text{exp}} = 155$ hr). Raw data were aggregated by averaging them over time steps of $\delta t = 1$ min. The reader is referred to Dhont (2017) and Dhont and Ancey (2018) for details of this experiment.

Figure 10a shows the bedload transport rate recorded at the flume outlet: Periods of intense bedload transport were usually associated with the destruction of gravel bars or the scouring of pools. Despite these pulses, the overall bedload transport rate behaved like a quasi-stationary process, as shown by Figure 10b. Applying the central limit theorem enabled us to estimate how the time-averaged mean and variance varied with sampling duration Δt, whereas the bootstrap method enabled us to generate double-averaged means and variances for different Δt values (see Figures 10c and 10d). Although the central limit theorem provides only an asymptotic expression for var $\overline{Q}_s$ (var $\overline{Q}_s = \sigma_q^2 \delta t/\Delta t$), we found that for all Δt values, this asymptotic relation closely matched the sample generated using the bootstrap method. Figure 10d shows that for a sampling
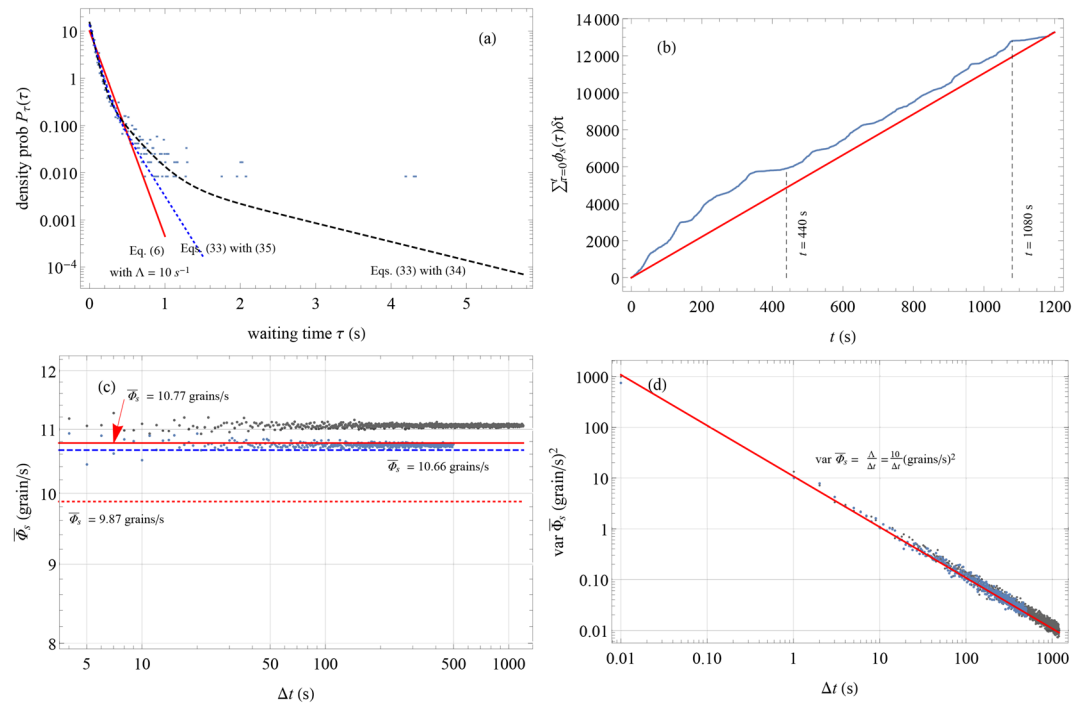
Figure 9. (a) Waiting time distribution at the flume outlet: Dots show the empirical probabilities. The solid red line is the exponential distribution (6) with rate $\widetilde{\Lambda} = 10.0$ grains/s. The dashed black line shows the hyperexponential distribution (33) fitted to the data. The dotted blue line shows the hyperexponential distribution (35) adjusted to the flume inlet data. (b) Stationarity test: Time variation in the cumulative number of particles crossing the control surface $\sum_{0}^{t} \varphi_s(\tau)\delta t$. The red line is the mean behavior $\hat{\Lambda} t$ with $\hat{\Lambda} = 13{,}271/1{,}200 = 11.06$ grains/s. The dashed vertical lines show the period (from 440 to 1,080 s) over which the particle flux could be considered stationary. (c) Variations in the double-averaged particle flux with the sampling duration Δt. The solid red line shows the mean particle flux $\hat{\Lambda}_r = N_r/640 = 10.77$ grains/s obtained by dividing the number of particles $N_r = 6{,}896$ leaving the flume between times $t = 440$ and $t = 1{,}080$ ss. The dashed red line shows the mean particle flux defined from the waiting time distribution by adjusting the exponential distribution (6) using the reduced sample, with $\widetilde{\Lambda}_r = 9.87$ grains/s. The dashed blue line shows the mean $\Phi_s = 10.66$ grains/s, computed using the renewal model (B11), with $p = 0.92$, $\lambda_1 = 3.59$ 1/s, $\lambda_2 = 14.69$ 1/s, $\alpha_1 = 0.16$, and $\alpha_2 = 0.84$. The blue points show the sample averages computed using the bootstrap method and the reduced sample as the training sample. The gray points show the sample averages when the entire time series is used as the bootstrap method's training sample. (d) Variation in the double-averaged variance var Φ_s with the sampling interval Δt. The solid red line shows the theoretical variance (9) with $\Lambda = \widetilde{\Lambda} = 10.0$ grains/s.

duration $\Delta t = 1$ min, the variance was 4.3 g^2/s^2, and thus we could only determine the mean bedload transport rate to within $\sqrt{4.3}/4.07 \sim 50\%$. If we wanted greater precision in the determination of Q_s—say 10% greater precision—we had to increase the sampling duration to 30 min, as per Figure 10d.

5.2. Gravel-Bed River

Here, we present an application to the River Navisence (canton Valais, Switzerland), a gravel-bed river near Zinal monitored since 2011. Bedload transport rates are measured using geophones placed across a concrete sill of width $W = 9$ m (Ancey et al., 2014; Wyss et al., 2016). The mean bed slope upstream of the sill is $i = 3.2\%$. The median particle diameter of transported bedload was $d_{50} = 8$ cm.

Figure 11a shows the time series of bedload transport rates Q_s and water discharge Q_w for 8 July 2012 (a day picked randomly). Water discharge varied throughout the day under the effect of sunshine. Overnight and in the morning, bedload transport rates were negligibly low. In the afternoon, ice melt and snow melt increased water discharge and thus the transport rate went up. We isolated a sequence of transport rates from 17:00 to 18:00, for which bedload transport could be considered stationary, as shown by Figure 11b.
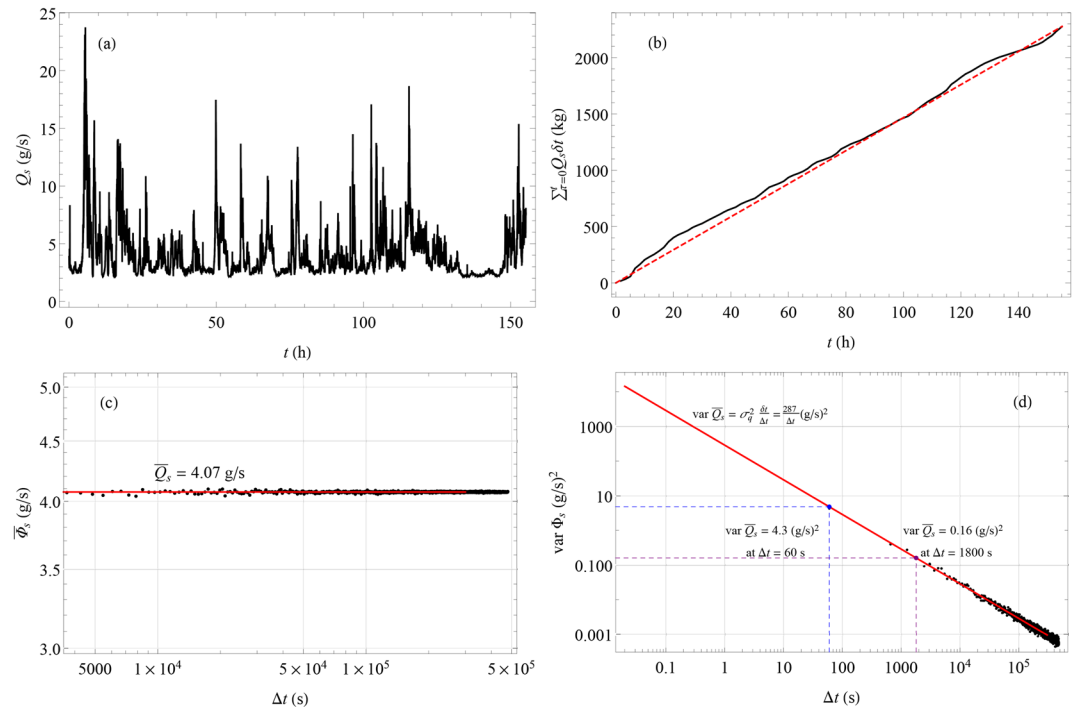
Figure 10. Application to a 19–m-long flume. (a) Time series of Φ_s. (b) Stationarity test. The dashed red line is the cumulative sediment mass $\int Q_s dt = \hat\Lambda t$ with $\hat\Lambda = 4.07$ g/s. (c) Variation in the double-averaged mean with the sampling duration Δt. The solid red line shows the mean flux $Q_{ss} = \hat\Lambda = 4.07$ g/s, whereas the black dots show the means generated using the bootstrap method. (d) Variation in the double-averaged variance with sampling duration Δt. The black dots show the variances generated using the bootstrap method. The solid red line is the theoretical variance $\mathrm{var}\, Q_s = \sigma_q^2 \delta t / \Delta t$ with $\sigma_q^2 = 4.8$ g^2/s^2.

Figures 11c and 11d show the double-averaged means and variances computed using the bootstrap method. As the bedload transport was stationary during the period considered, the double-averaged means were close to the mean rate $\overline{Q}_{ss} = \hat\Lambda = 236$ g/s estimated using the stationarity test (see Figure 11b). The variance curve in Figure 11d enabled us to estimate that for $\Delta t = \delta t = 60$ s, the mean transport rate was accurate to within $\sigma_q/\overline{Q}_s = 36\%$. Increasing Δt by a factor of 10 ($\Delta t = 10$ min) decreased the uncertainty to 3.6%. As the 17:00 to 18:00 time slot corresponded to the day's peak bedload transport activity, it is tempting to consider that a convenient sampling duration for 8 July 2012 was $\Delta t = 10$ min—sufficiently long to obtain low $\mathrm{var}\, \overline{Q}_s$ values and sufficiently short to capture the slow variations in the bedload transport rate with water discharge.

6. Conclusion

Bedload transport rates usually exhibit wide fluctuations, even under steady flow conditions. Measurements of time-averaged transport rates Q_s representative of bedload transport at given times can thus be biased to varying degrees, as illustrated by Figure 1, where errors exceeding 100% can be observed at certain sampling durations.

The present paper examines how we can assess the uncertainties associated with estimating a time-averaged transport rate $\overline{Q}_s$. We used the birth-death immigration-emigration model developed by Ancey et al. (2008). We arrive at an experimental protocol for measuring the mean particle flux $Q_s = \overline{\Phi}_s$ or bedload transport rate $Q_s = \overline{q}_s$ (see section 2.7) and estimating the uncertainties associated with that measurement. The first step is to define a time interval over which $Q_s(t)$ behaves like a stationary process. Depending on the data acquisition frequency and the relevance of the Markovian assumption (waiting times distributed exponentially or exhibiting a thicker tail), different models can be used to define the double-averaged mean and variance. When data-acquisition frequencies are sufficiently high (typically, higher than 1 Hz) and the Markovian
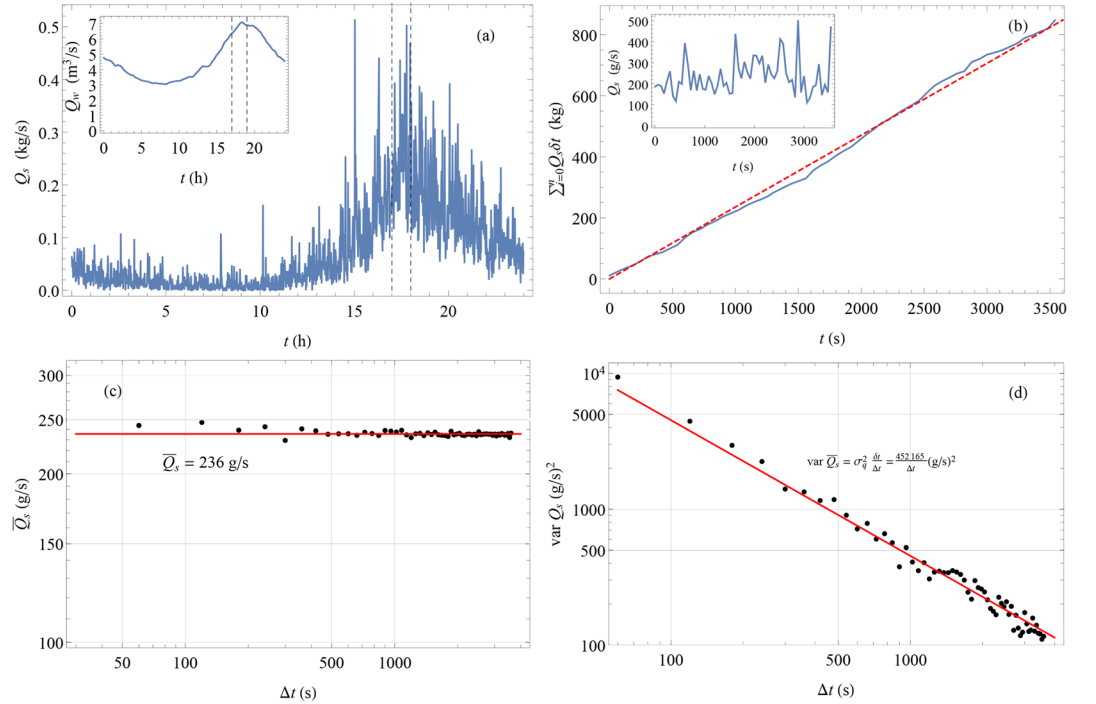
Figure 11. Application to the River Navisence. (a) Time series for 8 July 2012. The inset shows the time variations in the water discharge Q_w, while in the main graph, we have plotted the Q_s time series for 8 July 2012 (Q_s has been averaged over time steps of $\delta t = 1$ min (Ancey et al., 2014; Wyss et al., 2016). From this time series, we extracted a sample from 17:00 to 18:00 (represented by the vertical dashed lines). (b) Stationarity test. The dashed red line is the cumulative mass $\int Q_s dt = \hat{\Lambda} t$ with $\hat{\Lambda} = 236$ g/s. (c) Variation in the double-averaged mean with the sampling duration Δt. The solid red line shows the mean flux $Q_{ss} = \hat{\Lambda} = 236$ g/s, whereas the black dots show the means generated using the bootstrap method. (d) Variation in the double-averaged variance with sampling duration Δt. The black dots show the variances generated using the bootstrap method. The solid red line is the theoretical variance var $Q_s = \sigma_q^2 \delta t / \Delta t$ with $\sigma_q^2 = 7536$ g^2/s^2.

assumption is realistic, then the Markovian model developed by Ancey et al. (2008) can be applied. When the Markovian assumption fails, a renewal model can be used. At low data acquisition frequencies, the central limit theorem can be employed to find the double-averaged variance's dependence on the sampling duration Δt.

Markov process theory provides valuable insights into the behavior of $\mathcal{Q}_s$ fluctuations. One remarkable result is that the ensemble variance of $\mathcal{Q}_s$ is controlled solely by the sampling duration Δt and mean rate $\overline{\mathcal{Q}}_s$. As exemplified by the toy model in section 1.3, this ensemble variance offers a better estimate of the uncertainties associated with the measurement of $\overline{\mathcal{Q}}_s$ than does sample variance.

Appendix A: Integral of a Markov Process

A1. Theoretical Reminder: Master Equations and Other Definitions

We assume that the time variations in N can be described using Markov process theory (Gillespie, 1992). Between times t and $t+dt$, the N variation (called the *propagator*)

$$\Theta(dt; n, t) = N(t + dt) - N(t) \quad \text{given that} \quad N(t) = n, \tag{A1}$$

has the following probability density function (strictly speaking, the probability mass function as N is a discrete random variable):

$$\Pi(m|t; n, t) = \text{prob}\left(\Theta(dt; n, t) = m\right), \tag{A2}$$

with $m = 0$, 1, or -1 for a birth-death Markov process. The process can be also described by introducing

the jump probability $q(n,t;\tau)$, which is the probability that N varies by ± 1 at some instant between t and $t +\tau$. The Markovian assumption imposes that for infinitesimal time intervals, $q(n,t;dt) = a(n,t)dt$, where a is a positive function of n and t. The state probability $w(m|n,t)$ is the probability that upon jumping at time t, N takes the new value $n+m$. The propagator density Π and the functions a and w are related:

$$\Pi(m|t; n, t) = a(n, t)\mathrm{d}tw(m|n, t)+(1 - a(n, t)\mathrm{d}t)\delta_k(m, 0), \tag{A3}$$

where δ_k is the Kronecker delta function.

We also define the *consolidated characterizing function*:

$$W(m|n, t) = a(n, t)w(m|n, t), \tag{A4}$$

which can be interpreted as follows: $W\mathrm{d}t$ is the probability that the number of particles $N(t) = n$ jumps from n to $n+m$ in the time interval $\mathrm{d}t$. This function can be used in the *master equation*, that is, the governing equation for the probability of observing $N(t)$:

$$\frac{\partial}{\partial t}P(n, t|n_0, t_0) = \sum_{m=-1}^{m=+1} W(m|n - m, t)P(n - m, t|n_0, t_0)-W(-m|n, t)P(n, t|n_0, t_0), \tag{A5}$$

and if we define

$$W_+(n) = W(1|n, t) \quad \text{and} \quad W_-(n) = W(-1|n, t), \tag{A6}$$

which are the probabilities of gain or loss, respectively, then the master equation A5 can also be written as

$$\frac{\partial}{\partial t}P(n, t|n_0, t_0) = W_-(n + 1)P(n + 1, t|n_0, t_0)-W_+(n)P(n, t|n_0, t_0)+W_+(n - 1)P(n - 1, t|n_0, t_0)-W_-(n)P(n, t|n_0, t_0). \tag{A7}$$

It can be shown that the process is entirely determined by the functions (Gillespie, 1992):

$$a(n) = W_+ + W_- = \nu_{\mathrm{in}} + \lambda + (\nu_{\mathrm{out}} + \mu + \sigma)n \tag{A8}$$

where $a(n)\mathrm{d}t$ represents the probability that N varies within the time period $\mathrm{d}t$, and

$$v(n) = W_+ - W_- = \nu_{\mathrm{in}} + \lambda + (\mu - \sigma - \nu_{\mathrm{out}})n. \tag{A9}$$

Equivalently, we can work with the pairs of functions (W_+, W_-) or (a, v).

A2. Mean, Variance, and Covariance of $N(t)$

It can be shown that the mean number of moving particles $\langle N\rangle$ satisfies the differential equation (see Chapter 6 in Gillespie, 1992):

$$\frac{\mathrm{d}}{\mathrm{d}t}\langle N\rangle = v(\langle N\rangle) = W_+(\langle N\rangle)-W_-(\langle N\rangle), \tag{A10}$$

subject to the initial condition $\langle N\rangle(t_0) = N_0$. The variance of N is governed by

$$\frac{\mathrm{d}}{\mathrm{d}t}\mathrm{var}\, N = 2(\langle Nv(N)\rangle-\langle N\rangle\langle v(N)\rangle) + (\langle a(N)\rangle), \tag{A11}$$

subject to $\mathrm{var}\, N(t_0) = 0$. The time covariance is

$$\frac{\mathrm{d}}{\mathrm{d}t_2}\mathrm{cov}\,(N(t_1), N(t_2)) = \langle N(t_1)v(N(t_2))\rangle-\langle N(t_1)\rangle\langle v(N(t_2))\rangle, \tag{A12}$$

for $t_0 \le t_1 \le t_2$ and subject to the initial condition $\mathrm{cov}\,(N(t_1),N(t_1)) = \mathrm{var}\, N(t_1)$.

A3. Integral S of $N(t)$

The time integral S of N is defined as

$$S(t) = \int_{t_0}^{t} N(t)\mathrm{d}t. \tag{A13}$$

Its mean value is given by

$$\frac{\mathrm{d}}{\mathrm{d}t}\langle S\rangle = \langle N\rangle, \tag{A14}$$

whereas the time variations in the covariance $\mathrm{cov}(S,N) = \langle SN\rangle - \langle S\rangle\langle N\rangle$ obey the equation

$$\frac{\mathrm{d}}{\mathrm{d}t}\mathrm{cov}\,(S,\,N) = \mathrm{var}\,N + \langle Sv(N)\rangle - \langle S\rangle\langle v(N)\rangle, \tag{A15}$$

subject to $\mathrm{cov}(S,N) = 0$ at time $t = t_0$. The S variance is

$$\frac{\mathrm{d}}{\mathrm{d}t}\mathrm{var}\,S = 2\mathrm{cov}\,(S,\,N), \tag{A16}$$

subject to $\mathrm{var}\,S(t_0) = 0$. The covariance of S is the solution to

$$\mathrm{cov}\,(S(t_1),\,S(t_2)) = \mathrm{var}\,S(t_1) + 2\int_{t_1}^{t_2}\mathrm{cov}\,(S(t_1),\,N(\tau))\mathrm{d}\tau \tag{A17}$$

for $t_0 \leq t_1 \leq t_2$ and where the integrand is the solution to the differential equation

$$\frac{\mathrm{d}}{\mathrm{d}t_2}\mathrm{cov}\,(S(t_1),\,N(t_2)) = \langle S(t_1)v(N(t_2))\rangle - \langle S(t_1)\rangle\langle v(N(t_2))\rangle, \tag{A18}$$

for $t_0 \leq t_1 \leq t_2$. We refer the reader to Chapter 6 in Gillespie (1992) for the proofs.

A4. Moments of S

The mean time integral S is the solution to Equation A14

$$\langle S(t)\rangle = N_0 t_c(1 - e^{-t/t_c}) + \langle N\rangle_{\mathrm{ss}}\left(t - t_c(1 - e^{-t/t_c})\right). \tag{A19}$$

The solution to the covariance Equation A15

$$\frac{\mathrm{d}}{\mathrm{d}t}\mathrm{cov}\,(S,\,N) = \mathrm{var}\,N - \alpha\,\mathrm{cov}\,(S,\,N),$$

takes the form

$$\mathrm{cov}\,(S,\,N) = \frac{N_0\gamma}{\alpha^2}\left(e^{-2t/t_c} + e^{-t/t_c}(\alpha t - 1)\right) + \frac{\beta(1 - e^{-t/t_c})^2 + \gamma\langle N\rangle_{\mathrm{ss}}(1 - 2\alpha t e^{-t/t_c} - e^{-2t/t_c})}{2\alpha^2}, \tag{A20}$$

where $\gamma = v_{\mathrm{out}} + \sigma + \mu$ and $\alpha = v_{\mathrm{out}} + \sigma - \mu$. We find that the covariance tends to the limit

$$\mathrm{cov}_{\mathrm{ss}}(S,\,N) = \frac{\beta + \gamma\langle N\rangle_{\mathrm{ss}}}{2\alpha^2} = \frac{(\lambda + v_{\mathrm{in}})(v_{\mathrm{out}} + \sigma)}{(v_{\mathrm{out}} + \sigma - \mu)^3}. \tag{A21}$$

Using Equation A16, we deduce the variance of S by integrating the covariance $\mathrm{cov}(S,N)$. Asymptotically, this scales as

$$\text{var } S \propto \frac{\beta + \gamma \langle N \rangle_{\text{ss}}}{\alpha^2} t = \frac{(\lambda + \nu_{\text{in}})(\nu_{\text{out}} + \sigma)t}{(\nu_{\text{out}} + \sigma - \mu)^3}. \tag{A22}$$

By solving Equation A17, we find that the autocorrelation function of S is

$$\rho_s(\tau) = 1 + \frac{t_c}{\tau} \frac{(\nu_{\text{out}} + \sigma - \mu)^3}{(\lambda + \nu_{\text{in}})(\nu_{\text{out}} + \sigma)}(1 - e^{-\tau/t_c}). \tag{A23}$$

Appendix B: Time-Averaged Particle Flux: Renewal Theory

The Markovian assumption imposes strict conditions on the applicability of Equation 8. These are either an exponential distribution for the waiting times or, equivalently, a Poisson process for the number of particles crossing the control surface. We can relax these assumptions by considering other probability distributions and using renewal theory to compute the number of particles crossing the control surface $\mathcal{S}$. Let us consider that one or two particles can arrive at the same time:

$$\text{prob } (N = 1) = p, \tag{B1}$$

$$\text{prob } (N = 2) = 1 - p, \tag{B2}$$

$$\text{prob } (N > 2) = 0, \tag{B3}$$

and that the waiting-time distribution is the two-parameter hyperexponential distribution, whose density function is

$$P_\tau(\tau) = \alpha_1 \lambda_1 \exp(-\lambda_1 \tau) + \alpha_2 \lambda_2 \exp(-\lambda_2 \tau), \tag{B4}$$

where α_1 and α_2 are mixture parameters satisfying $\alpha_1 + \alpha_2 = 1$, whereas λ_1 and λ_2 are two rates. At time t, M jumps have occurred (with one or two arrivals). Let us call S the sum of particles that have crossed the control surface up to time t

$$S(t) = \sum_{i=1}^{M(t)} N_i \tag{B5}$$

where $M(t) = \max\{n : T_n \leq t\}$, and $T_n = \tau_1 + \tau_2 + ... + \tau_n$ for $n \geq 1$ ($T_0 = 0$), and τ_i is a sequence of waiting times distributed from (B4). There is no analytical expression of S in (B5), but we can derive approximations in the limit of $t \to \infty$. Using Wald's equation (Grimmett & Stirzaker, 2008), we can deduce the expectation of the sum S:

$$\mathbb{E}(S) = \mathbb{E}(N)\mathbb{E}(M), \tag{B6}$$

and using the law of total variance, we get its variance:

$$\text{var } S = \text{var } N \mathbb{E}(M) + \mathbb{E}(N)^2 \text{var } M. \tag{B7}$$

Here we have: $\text{var } N = p(1-p)$ and $\mathbb{E}(N) = 2 - p$. The number of jumps can be approximated as follows:

$$\mathbb{E}(M) = \frac{t}{\bar{\tau}} + o(t), \tag{B8}$$

$$\text{var } M = \frac{t \sigma_\tau^2}{\bar{\tau}^3} + o(t), \tag{B9}$$

with

$$\bar{\tau} = \frac{\alpha_1}{\lambda_1} + \frac{\alpha_2}{\lambda_2} \quad \text{and} \quad \sigma_\tau^2 = 2\left(\frac{\alpha_1}{\lambda_1^2} + \frac{\alpha_2}{\lambda_2^2}\right) - \left(\frac{\alpha_1}{\lambda_1} + \frac{\alpha_2}{\lambda_2}\right)^2. \tag{B10}$$

We then deduce:

$$\overline{\Phi}_s(t) = \mathbb{E}\left(\frac{S}{t}\right) = (2 - p)\frac{\lambda_1\lambda_2}{\lambda_2\alpha_1 + \lambda_1\alpha_2}, \tag{B11}$$

and

$$\text{var}\,\Phi_s(t) = \text{var}\left(\frac{S}{t}\right) = \left(\frac{p(1-p)}{\bar{\tau}} + \frac{(2-p)^2\text{var}\,\tau}{\bar{\tau}^3}\right)\frac{1}{t}. \tag{B12}$$

Appendix C: Exponential Velocity Distribution

Let us consider that the particle velocity is distributed exponentially. We then replace the Gaussian distribution (5) with the exponential law with mean $\bar{u}_p$

$$P_u(w) = \text{prob}(u = w) = \frac{1}{\bar{u}_p}\exp(-w/\bar{u}_p). \tag{C1}$$

Like in section 2.5, we introduce the sum of k particle velocities

$$U = \sum_{i=1}^{k} u_{p,i}. \tag{C2}$$

If k is fixed, then the probability P_k of observing U is the Erlang distribution with shape k and rate $1/\bar{u}_p$. If k varies randomly, then the probability of observing U is

$$P_U = \sum_{k=1}^{\infty} P_n(k)P_k(U). \tag{C3}$$

The volume-averaged transport rate is $q_s = U/L$. If we still assume that the probability of observing k particles is given by the negative binomial distribution with parameters p and q, the probability distribution of U becomes

$$P_{q_s} = LP_U(Lq_s) = L\sum_{k=1}^{\infty}\binom{q+n-1}{q-1}p^q(1-p)^n\frac{(Lq_s)^{k-1}e^{-Lq_s/\bar{u}_p}}{\bar{u}_p^k(k-1)!}. \tag{C4}$$

There exists a closed-form expression for P_{q_s}, but we just need the first two moments:

$$\langle q_s \rangle = \int_{\mathbb{R}_+} q_s P_{q_s}\,\mathrm{d}q_s = \frac{N_{\text{ss}}}{L}\bar{u}_p, \tag{C5}$$

$$\text{var}\,q_s = \int_{\mathbb{R}_+}(q_s - \langle q_s \rangle)^2 P_{q_s}\,\mathrm{d}q_s = \frac{\text{var}_{\text{ss}}N}{L^2}(1+p)\bar{u}_p^2. \tag{C6}$$

Assuming that particle velocity and particle number are independent variables, we can generalize the variance Equation 18 to take velocity fluctuations into account in the double-averaged variance by following the same reasoning as that used for deriving Equation 18:

$$\text{var}\,\overline{q}_s(\Delta t|t) = \text{var}_{ss}N\frac{\bar{u}_p^2}{L^2}(1+p)\frac{t_c}{\Delta t}, \tag{C7}$$

an expression that is close to Equation 25 obtained for Gaussian velocity distributions.

Notation

Here we provide the list of variables used in the paper, their meaning, and physical units.

D deposition rate [grains s^{-1}]

d_{50} mean particle diameter [m]

E entrainment rate [grains s^{-1}]

L control window's length [mm]

M number of samples

N, n number of moving particles

p parameter of the Bernoulli distribution

P probability density function

P_n probability density function of N

P_q probability density function of q_s [s]

P_u probability density function of particle velocity [s m^{-1}]

P_τ probability density function of waiting time [s^{-1}]

q parameter of the negative Bernoulli distribution

q_s instantaneous particle transport rate [grains s^{-1}]

Q_s instantaneous particle transport rate [g s^{-1}]

Q_w water discharge [L s^{-1}]

S time integral of $N(t)$

$\mathscr{S}$ control surface

S_n sum of n variables

t time [s]

t_i discrete time [s]

t_c autocorrelation time [s]

$\mathscr{U}_p$ volume-averaged particle velocity [m s^{-1}]

$\bar{u}_p$ mean particle velocity [m s^{-1}]

$\mathscr{V}$ control volume

x streamwise coordinate [m]

y random variable

α_i mixture coefficient

δt time interval [s]

Δt sampling duration [s]

φ_s particle arrival rate [grains s^{-1}]

Φ_s particle flux [grains s^{-1}]

λ entrainment rate [grains s^{-1}]

λ_i Poisson rate [s^{-1}]

Λ Poisson rate [grains s^{-1}]

μ collective entrainment rate [s^{-1}]

ν_{in} mean particle flux [grains s^{-1}]

ν_{out} emigration rate [s^{-1}]

ρ autocorrelation function

σ deposition rate [s^{-1}]

σ_u particle velocity's standard deviation [m s^{-1}]

σ_q standard deviation of q_s [g s^{-1} or grains s^{-1}]

τ waiting time[s]

Data Availability Statement

The Mathematica scripts and data used for computing Figures 1 to 10 are available from the *figshare* data repository (https://doi.org/10.6084/m9.figshare.11513073).

References

Ancey, C. (2010). Stochastic approximation of the Exner equation under lower-regime conditions. *Journal of Geophysical Research*, *115*, F00A11. https://doi.org/10.1029/2009JF001260

Ancey, C. (2020). Bedload transport: A walk between randomness and determinism. Part 2: Challenges and prospects. *Journal of Hydraulic Research*, *58*, 18–33.

Ancey, C., Bohorquez, P., & Bardou, E. (2014). Sediment transport in mountain rivers. *Ercoftac*, *89*, 37–52.

Ancey, C., Davison, A. C., Böhm, T., Jodeau, M., & Frey, P. (2008). Entrainment and motion of coarse particles in a shallow water stream down a steep slope. *Journal of Fluid Mechanics*, *595*, 83–114.

Ancey, C., & Heyman, J. (2014). A microstructural approach to bed load transport: Mean behaviour and fluctuations of particle transport rates. *Journal of Fluid Mechanics*, *744*, 129–168.

Ballio, F., Nikora, V., & Coleman, S. (2014). On the definition of solid discharge in hydro-environment research and applications. *Journal of Hydraulic Research*, *52*, 173–184. https://doi.org/10.1002/2016jf004087

Ballio, F., Pokrajac, D., Radice, A., & Hosseini Sadabadi, S. A. (2018). Lagrangian and Eulerian description of bed-load transport. *Journal of Geophysical Research: Earth Surface*, *123*, 384–408. https://doi.org/10.1002/2016JF004087

Bunte, K., & Abt, S. (2005). Effect of sampling time on measured gravel bed load transport rates in a coarse-bedded stream. *Water Resources Research*, *41*, W11405. https://doi.org/10.1029/2004WR003880

Campagnol, J., Radice, A., & Ballio, F. (2012). Scale-based statistical analysis of sediment fluxes. *Acta Geophysica*, *60*, 1744–1777.

Cox, D., & Miller, H. (1965). *The theory of stochastic processes*. Boca Raton: Chapman & Hall CRC.

Cudden, J., & Hoey, T. B. (2003). The causes of bedload pulses in a gravel channel: The implications of bedload grain-size distributions. *Earth Surface Processes and Landforms*, *28*, 1411–1428.

Davison, A. C., & Hinkley, D. V. (1997). *Bootstrap methods and their application*. Cambridge: Cambridge University Press.

Dhont, B. (2017). *Sediment pulses in a gravel-bed flume with alternate bars*. École Polytechnique Fédérale de Lausanne.

Dhont, B., & Ancey, C. (2018). Are bedload transport pulses in gravel-bed rivers created by bar migration or sediment waves? *Geophysical Research Letters*, *45*, 5501–5508. https://doi.org/10.1029/2018GL077792

Dhont, B., Rousseau, G., & Ancey, C. (2017). Continuous monitoring of bedload transport in a laboratory flume using an impact sensor. *Journal of Hydraulic Engineering*, *143*, 04017005.

Dietze, M., Lagarde, S., Halfi, E., Laronne, J., & Turowski, J. M. (2019). Joint sensing of bedload flux and water depth by seismic data inversion. *Water Resources Research*, *55*, 9892–9904. https://doi.org/10.1029/2019WR026072

Drew, D., & Passman, S. (1999). *Theory of multicomponent fluids*. New York: Springer.

Einstein, H. (1950). *The bed-load function for sediment transportation in open channel flows (Technical Report No. 1026)*. United States Department of Agriculture.

Furbish, D., Fathel, S. L., & Schmeeckle, M. W. (2017). Particle motions and bedload transport theory: The entrainment forms of the flux and the Exner equation. In D. Tsutsumi, & J. B. Laronne (Eds.), *Gravel-Bed Rivers: Processes and Disasters* (pp. 97–120). Chichester: John Wiley & Sons.

Furbish, D., Haff, P., Roseberry, J., & Schmeeckle, M. (2012). A probabilistic description of the bed load sediment flux: 1. Theory. *Journal of Geophysical Research*, *117*, F03031. https://doi.org/10.1029/2012JF002352

Geay, T., Belleudy, P., Gervaise, C., Habersack, H., Aigner, J., Kreisler, A., et al. (2017). Passive acoustic monitoring of bedload discharge in a large gravel bed river. *Journal of Geophysical Research: Earth Surface*, *122*, 528–545. https://doi.org/10.1002/2016JF004112

Gillespie, D. (1992). *Markov processes: An introduction for physical scientists*. San Diego: Academic Press.

Gomez, B. (1991). Bedload transport. *Earth-Science Reviews*, *31*, 89–132.

Gray, J. R., Laronne, J., & Marr, J. (2010). *Bedload-surrogate monitoring technologies (Vols Scientific Investigations Report 2010–5091)*. Reston, VA: US Department of the Interior, US Geological Survey.

Grimmett, G., & Stirzaker, D. (2008). *Probability and random processes* (3rd ed.). Oxford: Oxford University Press.

Herczynski, R., & Pienkowska, I. (1980). Toward a statistical theory of suspension. *Annual Review of Fluid Mechanics*, *12*, 237–269.

Heyman, J., Bohorquez, P., & Ancey, C. (2016). Entrainment, motion, and deposition of coarse particles transported by water over a sloping mobile bed. *Journal of Geophysical Research: Earth Surface*, *121*, 1931–1952. https://doi.org/10.1002/2015JF003672

Jaqaman, K., Loerke, D., Mettlen, M., Kuwata, H., Grinstein, S., Schmid, S. L., & Danuser, G. (2008). Robust single-particle tracking in live-cell time-lapse sequences. *Nature Methods*, *5*(8), 695.

Lajeunesse, E., Malverti, L., & Charru, F. (2010). Bed load transport in turbulent flow at the grain scale: Experiments and modeling. *Journal of Geophysical Research*, *115*, F04001. https://doi.org/10.1029/2009JF001628

Lhuillier, D. (1992). Ensemble averaging in slightly non-uniform suspensions. *European Journal of Mechanics B/Fluids*, *6*, 649–661.

Martin, R., Jerolmack, D., & Schumer, R. (2012). The physical basis for anomalous diffusion in bed load transport. *Journal of Geophysical Research*, *117*, F01018. https://doi.org/10.1029/2011JF002075

Mendes, L., Antico, F., Sanches, P., Alegria, F., Aleixo, R., & Ferreira, R. (2016). A particle counting system for calculation of bedload fluxes. *Measurement Science and Technology*, *27*(12), 125,305.

Recking, A. (2013). Simple method for calculating reach-averaged bed-load transport. *Journal of Hydraulic Engineering*, *139*, 70–75.

Recking, A., Liébault, F., Peteuil, C., & Jolimet, T. (2012). Testing bedload transport equations with consideration of time scales. *Earth Surface Processes and Landforms*, *37*, 774–789.

Rickenmann, D., Turowski, J. M., Fritschi, B., Wyss, C., Laronne, J. B., Barzilai, R., et al. (2014). Bedload transport measurements with impact plate geophones: Comparison of sensor calibration in different gravel-bed streams. *Earth Surface Processes and Landforms*, *39*, 928–942.

Roseberry, J., Schmeeckle, M., & Furbish, D. (2012). A probabilistic description of the bed load sediment flux: 2. Particle activity and motions. *Journal of Geophysical Research*, *117*, F03032. https://doi.org/10.1029/2012JF002353

Seizilles, G., Lajeunesse, E., Devauchelle, O., & Bak, M. (2014). Cross-stream diffusion in bedload transport. *Physics of Fluids*, *26*, 013302.

Singh, A., Fienberg, K., Jerolmack, D., Marr, J., & Foufoula-Georgiou, E. (2009). Experimental evidence for statistical scaling and intermittency in sediment transport rates. *Journal of Geophysical Research*, *114*, F01025. https://doi.org/10.1029/2007JF000963

Tinevez, J.-Y., Perry, N., Schindelin, J., Hoopes, G. M., Reynolds, G. D., Laplantine, E., et al. (2017). TrackMate: An open and extensible platform for single-particle tracking. *Methods*, *115*, 80–90.

Tsakiris, A., Papanicolaou, A. N., & Lauth, T. (2014). Signature of bedload particle transport mode in the acoustic signal of a geophone. *Journal of Hydraulic Research*, *52*, 185–204.

Wilcock, P. (1997). Entrainment, displacement and transport of tracer gravels. *Earth Surface Processes and Landforms*, *22*, 1125–1138.

Wyss, C. R., Rickenmann, D., Fritschi, B., Turowski, J. M., Weitbrecht, V., Travaglini, E., et al. (2016). Laboratory flume experiments with the Swiss plate geophone bedload monitoring system. Part II: Application to field sites with direct bedload samples. *Water Resources Research*, *52*, 7760–7778. https://doi.org/10.1002/2016WR019283